Inferring the dynamical effects of stroke lesions through whole-brain modeling

Sebastian Idesis [a,*], Chiara Favaretto [b,c], Nicholas V. Metcalf [d], Joseph C. Griffis [d], Gordon L. Shulman [d,e], Maurizio Corbetta [b,c,d,e,f], Gustavo Deco [a,g]

[a] Center for Brain and Cognition (CBC), Department of Information Technologies and Communications (DTIC), Pompeu Fabra University, Edifici Mercè Rodoreda, Carrer Trias i Fargas 25-27, Barcelona, Catalonia 08005, Spain
[b] Padova Neuroscience Center (PNC), University of Padova, via Orus 2/B, Padova 35129, Italy
[c] Department of Neuroscience (DNS), University of Padova, via Giustiniani 2, Padova 35128, Italy
[d] Department of Neurology, Washington University School of Medicine, 660 S. Euclid Ave, St. Louis, MO 63110, USA
[e] Department of Radiology, Washington University School of Medicine, 660 S. Euclid Ave, St. Louis, MO 63110, USA
[f] VIMM, Venetian Institute of Molecular Medicine (VIMM), Biomedical Foundation, via Orus 2, Padova 35129, Italy
[g] Institució Catalana de Recerca I Estudis Avançats (ICREA), Passeig Lluis Companys 23, Barcelona, Catalonia 08010, Spain

ARTICLE INFO

ABSTRACT

Understanding the effect of focal lesions (stroke) on brain structure-function traditionally relies on behavioral analyses and correlation with neuroimaging data. Here we use structural disconnection maps from individual lesions to derive a causal mechanistic generative whole-brain model able to explain both functional connectivity alterations and behavioral deficits induced by stroke. As compared to other models that use only the local lesion information, the similarity to the empirical fMRI connectivity increases when the widespread structural disconnection information is considered. The presented model classifies behavioral impairment severity with higher accuracy than other types of information (e.g.: functional connectivity). We assessed topological measures that characterize the functional effects of damage. With the obtained results, we were able to understand how network dynamics change emerge, in a nontrivial way, after a stroke injury of the underlying complex brain system. This type of modeling, including structural disconnection information, helps to deepen our understanding of the underlying mechanisms of stroke lesions.

1. Introduction

In the last two centuries, the study of patients with focal brain lesions has been the main approach for understanding brain organization and localization of function (Bates et al., 2001; Broca, 1861; Corbetta et al., 2015; Karnath et al., 2018; Mesulam, 1981). More recently, nonetheless, it has become apparent that focal lesions cause widespread abnormalities of brain network activity that correlate with cognitive deficits and recovery of function (Corbetta et al., 2018; He et al., 2007; Ovadia-Caro et al., 2013; Siegel et al., 2016; Wang et al., 2019). In parallel new methods have been developed to map lesion-related patterns of disconnection, either structural (Foulon et al., 2018) or functional (Boes, 2015), not directly, but using clinical scans and normative connectomes. However, which signals provide the most accurate prediction of cognitive impairments and recovery of function remains controversial

(Bowren et al., 2022; J. C. Griffis et al., 2019; Salvalaggio et al., 2020; Weiss Cohen & Regazzoni, 2020).

Correlational studies such as those discussed above do not provide a clear mechanistic understanding of how brain lesions affect information processing. A recent development -whole-brain models- use biologically plausible structural connectivity coupled with a local model of activity as the input for the generation of global dynamics, and can thus be used to understand the effect of damage on global (whole brain) dynamics (Adhikari et al., 2017; Cabral et al., 2012; Cofré et al., 2020; Kringelbach et al., 2020; Saenger et al., 2018). Early attempts used volume and location information to modify a healthy structural connectome to approximate the effect of lesions and fitted the yielded global dynamics to the patient's own blood oxygenation level-dependent (BOLD) signals measured with functional magnetic resonance imaging (fMRI) (Adhikari et al., 2017; Saenger et al., 2018). These studies showed that focal

lesions cause a decrease in both segregation and integration at rest, as well as a decrease in neural state variability or entropy during stimulation.

In this study, we innovate whole-brain models of stroke lesions in two ways.

First, we optimize the whole brain model (Deco et al., 2017; Jobst et al., 2017) by converting it into a generative model to yield Effective Connectivity (EC). We described the model as 'generative' since the underlying BOLD signals are generated from the model. In contrast to functional connectivity (FC) that describes the statistical interactions between regions, and structural connectivity (SC) that describes the undirected anatomical links between two brain regions, EC describes causal pairwise interactions that show the influence one region exerts over another in a directed way (Gilson et al., 2016). EC links are directional and provide information on asymmetrical regional pairwise temporal interactions. Second, crucially, we take into consideration the effect of lesions on the structural connectome that are driven by direct damage to the white matter, rather than focusing solely on the connections of damaged grey matter regions. On average, a stroke is expected to cause disconnection in about 20 % of all brain connections based on diffusion imaging connectomes (Joseph C Griffis et al., 2019a). Moreover, lesions that directly disconnect brain regions and/or interrupt intermediate links between brain regions are the main sources of FC abnormalities after stroke (J. C. Griffis et al., 2019; Griffis et al., 2021). Hence, the whole brain model is adjusted in terms of its input connectivity by the pattern of SC disconnection computed in each patient.

To validate the use of EC whole-brain models, we compare EC to SC or FC models for the prediction of stroke-related deficits. Recent studies have reported a higher predictive value of EC over FC in normal or pathological conditions, such as epilepsy or addiction (Hejazi & Nasrabadi, 2019; Pallarés et al., 2018; Wei et al., 2021). Other studies have used machine learning to compare the prediction of neurological deficits (motor, language, attention, etc.) based respectively on lesion location, SC, or FC disconnection computed indirectly in normative atlases (Pini et al., 2021; Salvalaggio et al., 2020). These studies found fairly accurate good predictions for lesion and SC disconnection, but not for FC disconnection. More clinically oriented studies have applied automatic classification methods to grade the severity of the stroke lesion (Acharya et al., 2019; Govindarajan et al., 2020; Sprigg et al., 2007).

In the current study, we implemented a classifier to distinguish the performance of stroke patients on different neuropsychological tasks by comparing prediction accuracy based on SC, FC, or EC models. Furthermore, by taking advantage of the asymmetric property of the EC, we measured the topology of graph measures in healthy and stroke patients. Treating the whole-brain models as a complex cluster of networks with nodes and edges characterized by global integration and local specialization (Tononi et al., 1994), we measured changes in graph topology to understand how network dynamics change after a stroke injury (Adhikari et al., 2021a; Vecchio et al., 2019a). Overall, the results show the importance of white matter structural disconnection for the accuracy of whole brain models of dynamics in stroke.

2. Methods

2.1. Subjects

We used the Washington University Stroke Cohort dataset (Corbetta et al., 2015), a large prospective longitudinal (two weeks, three months, 12 months) study of first-time single lesion stroke in different locations. The database includes patients with first-time stroke, studied at 1–2 weeks (mean = 13.4 days, SD = 4.8 days), 3 months, and 12 months after stroke onset. For the current study, only the first time point was considered (2 weeks after stroke) excluding from the analysis the other 2 time points (3 months and 12 months). Furthermore, a group of age-matched control subjects was evaluated twice at an interval of three months. Being a cross-sectional analysis, from this cohort we selected 96

S patients and 27 healthy subjects.

Stroke patients were prospectively recruited from the stroke service at Barnes-Jewish Hospital (BJH), with the help of the Washington University Cognitive Rehabilitation Research Group (CRRG). The complete data collection protocol is described in full detail in a previous publication (Corbetta et al., 2015). Healthy controls were selected based on the same inclusion/exclusion criteria as in (Corbetta et al., 2015). This group is typically constituted of spouses or first-degree relatives of the patients, age- and education-matched to the stroke sample. Patients were characterized with a robust neuroimaging battery for structural and functional features, and an extensive (~2 h) neuropsychological battery.

2.2. Neuroimaging acquisition and preprocessing

A complete description of the neuroimaging assessment is given in (J. C. Griffis et al., 2019). Neuroimaging data were collected at the Washington University School of Medicine using a Siemens 3T Tim-Trio scanner with a 12-channel head coil, specifically: 1) sagittal T1-weighted MP-RAGE (TR = 1950 msec; TE = 2.26 msec, flip angle = 90 degrees; voxel dimensions = 1.0x1.0x1.0 mm), and 2) a gradient echo *EPI* (TR = 2000 msec; TE = 2 msec; 32 contiguous slices; 4x4 mm in-plane resolution) resting-state functional MRI scans from each subject. Participants were instructed to fixate on a small centrally located white fixation cross that was presented against a black background on a screen at the back of the magnet bore. Between six and eight resting-state scans (128 volumes each) were obtained from each participant (~30 min total) giving a total of 896 time points for each participant.

Resting-state fMRI preprocessing included (i) regression of head motion, signal from ventricles and CSF, signal from white matter, global signal (ii) temporal filtering retaining frequencies in 0.009–0.08 Hz band: and (iii) frame censoring, FD = 0.5 mm. Finally, the resulting residual time series were projected on the cortical and subcortical surface of each subject divided into 235 ROIs (200 cortical plus 35 subcortical). These areas were taken from the multi-resolution functional connectivity-based cortical parcellations developed by Schaefer and colleagues (Schaefer et al., 2018), including additional subcortical and cerebellar parcels from the Automated Anatomical Labeling (AAL) atlas (Tzourio-Mazoyer et al., 2002) and a brainstem parcel from the Harvard-Oxford Subcortical atlas (https://fsl.fmrib.ox.ac.uk/fsl/fslwiki/Atlases).

A structural connectome atlas was created using a publicly available diffusion MRI streamline tractography atlas based on high angular resolution diffusion MRI data collected from 842 healthy Human Connectome Project participants (Yeh et al., 2018) as described previously (Griffis et al., 2019, 2021). Briefly, the HCP-842 atlas was built using high spatial and high angular resolution diffusion MRI data collected from N = 842 healthy Human Connectome Project participants. These data were reconstructed in the MNI template space using q-space diffeomorphic reconstruction (Yeh & Tseng, 2011), and the resulting spin distribution functions were averaged across all 842 individuals to estimate the normal population-level diffusion patterns. Whole-brain deterministic tractography was then performed on the population-averaged dataset using multiple turning angle thresholds to obtain 500,000 population-level streamline trajectories.

2.3. Neuropsychological and behavioral assessment

The same subjects (controls and patients) underwent a battery of neuropsychological tests in the domains of motor, attention, language, visual, and memory functions at each time point. Briefly, the battery consisted of 44 measures across four domains of function: language, motor attention, and memory (for a complete description of the tasks measures, see (Corbetta et al., 2015). A dimensionality reduction was applied to the individual test data in each domain using principal component analysis as in (Corbetta et al., 2015), yielding summary

domain scores: Language, MotorR and MotorL (one score per side of the body), AttentionVF (visuospatial field bias), Average performance (overall performance and reaction times on attention tasks), and AttentionValDis (the ability to re-orient attention to unattended stimuli), Memory V (composite verbal memory score) and MemoryS (composite spatial memory score). Finally, patients' behavioral scores were z-scored with regard to controls' scores, to highlight behavioral impairments.

In addition to domain-specific scores, the patients' clinical severity was assessed through the National Institutes of Health Stroke Scale (NIHSS) (Brott et al., 1989) which includes 15 subtests addressing: level of consciousness (LOC), gaze and visual field deficits, facial palsy, upper and lower motor deficits, limb ataxia, sensory impairment, inattention, dysarthria and language deficits. The total NIHSS score was used as an averaged measure of the clinical severity for each patient.

2.4. Neuroimaging features for classification

2.4.1. Lesions

Each lesion was manually segmented on structural MRI scans and checked by two board-certified neurologists. The location (cortico-subcortical, subcortical, white-matter only) of each lesion was assigned with an unsupervised K-means clustering on the percentage of total cortical/subcortical gray and white matter masks overlay. For a more extensive explanation of how the overlap of each lesion group with gray matter, white matter, and subcortical nuclei is calculated, see Corbetta et al, 2015.

2.4.2. FC measures

Based on previous work (J. C. Griffis et al., 2019; Siegel et al., 2016) we defined three measures that are consistently impaired in stroke patients:

1. Intra-hemispheric FC: average between pairwise FC of Dorsal attention network (DAN) and Default mode network (DMN) regions.
2. Inter-hemispheric FC: average homotopic inter-hemispheric connectivity within each network
3. Modularity: overall Newman's modularity among cortical networks, a comparison between the number of connections within a module to the number of connections between modules (Newman & Girvan, 2004)

2.4.3. Lesion disconnection masks

The Lesion Quantification Toolkit (Griffis et al., 2021) produces a comprehensive set of atlas-derived lesion measures that include measures of grey matter damage, white matter disconnection, and alterations of higher-order brain network topology. Importantly, the measures produced by the toolkit are based on population-scale (e.g. N = 842) atlases of grey matter parcel boundaries and white matter connection trajectories that were constructed from high-quality resting-state functional MRI and diffusion MRI data using state-of-the-art methods.

Taking advantage of the Lesion Quantification Toolkit (LQT), the structural disconnection (SDC) masks consisted of a spared connection adjacency matrix where each cell quantified the percent of streamlines connecting each region pair in the atlas-based structural connectome that were spared by the lesion. Therefore, the multiplication of each SDC with a template SC provides an atlas-based weight for each region pair corresponding to each patient. For the mentioned cohort, DTI was not acquired during the subacute stage visit (~2 weeks), only during the two subsequent chronic visits (not included in the current study). Therefore, the estimates from the LQT were used.

In addition, for the analysis of the FC impairments metrics, a second mask, based on gray matter damage, was tested as a control (gray matter in Fig. 2). Inspiredby a previous study (Adhikari et al., 2017) we applied a disconnection mask measuring all connections incoming or outgoing

from the damaged cortical parcels. In other words, the mask for each patient included all links observed in healthy controls except, those from and to a node with 100 % grey matter damage (Adhikari et al., 2021b). The two masks, therefore, capture damage of white matter connections to/from the damaged gray matter or capture more directly the disconnection induced by both gray matter and white matter damage. Since many stroke lesions occur predominantly in the white matter or include both a gray and white matter component, the SDC mask shall provide a more accurate description of the damage to the connectome. It is important to realize that for the lesions that were only subcortical, no gray matter damage was computed revealing a huge limitation of the gray matter mask.

2.5. Whole-brain Hopf model parameter estimation

We simulated the BOLD activity at the whole-brain level by using the so-called Hopf computational model, which simulates the dynamics emerging from the mutual interactions between brain areas, considered to be interconnected based on the established graphs of anatomical SC (Deco et al., 2017; Kringelbach et al., 2015). The structural connectivity matrix was scaled to a maximum value of 0.2 (Deco et al., 2017), leading to a reduction of the parameter space to search for the optimal parameter. We calculated the global scale factor, G coupling value, which assesses the influence of the SC in the model. We selected the optimal value in which the model phases were more like the empirical data. The model consists of 235 coupled dynamical units (ROIs or nodes) representing the 200 cortical and 35 subcortical brain areas from the parcellation. The local dynamics of each brain area (node) is described by the normal form of a supercritical Hopf bifurcation, also called a Landau–Stuart oscillator, which is the canonical model for studying the transition from noisy to oscillatory dynamics (Kuznetsov, 1998). When coupled together using brain network anatomy (Explained above in the "Neuroimaging acquisition and preprocessing" section), the complex interactions between Hopf oscillators have been shown to successfully replicate features of brain dynamics observed in fMRI (Deco et al., 2017; Kringelbach et al., 2015).

The local dynamics of each individual node is described by the normal form of a supercritical Hopf bifurcation, which is able to describe the transition from asynchronous noisy behavior to full oscillations. Thus, in complex coordinates, each node j is described by the following equation: (For more information, see Deco et al., 2019).

$$\frac{dz_j}{dt} = z(a_j + i\omega_j - |z_j|^2) + g\sum_{k=1}^{N} C_{jk}(z_k - z_j) + \beta\eta_j, \qquad (1)$$

Where

$$z_j = p_j e^{i\theta} = x_j + iy_j \qquad (2)$$

α and ω are the bifurcation parameters and the intrinsic frequencies of the system, respectively. This normal form has a supercritical bifurcation at $a_j = 0$. Within this model, the intrinsic frequency ω_j of each node is in the 0.04–0.07 Hz band (i = 1, …, n). The intrinsic frequencies were estimated from the data, as given by the averaged peak frequency of the narrowband BOLD signals of each brain region. The variable g represents a global coupling scaling the structural connectivity C_{jk}, and η is a Gaussian noise vector with standard deviation $\beta = 0.04$. This model can be interpreted as an extension of the Kuramoto model with amplitude variations, hence the choice of coupling $(z_k - z_j)$, which relates to a tendency of synchronization between two coupled nodes. We insert Eq. (2) in Eq. (1) and separate the real part in Eq. (3) and the imaginary part in Eq. (4) (Deco et al., 2017).

$$\frac{dx_j}{dt} = \left(a_j - x_j^2 - y_j^2\right)x_j - \omega_j y_j + G\sum_{i} C_{jk}(\chi_i - x_j)\beta\eta_j(\tau) \qquad (3)$$

$$\frac{dy_j}{dt} = \left(a_j - x_j^2 - y_j^2\right)y_j - \omega_j x_j + G\sum_i C_{jk}\left(y_i - y_j\right)\beta\eta_j(\tau) \tag{4}$$

It is important to clarify that for the EC + SDC model, the SDC information was added to the structural connectivity in order to enhance the optimization of it (See "Lesion disconnection masks" section).

2.6. Effective connectivity calculation

The analysis of EC incorporates an indirect metric (as it is derived from other presented metrics) into the whole-brain model to replace the existing descriptive metrics of FC and SC. Previous studies have shown how EC is fundamental to understand the propagation of information in structural networks (Gilson et al., 2016; Jobst et al., 2017). Methods for estimating EC are explained in detail in a previous publication (Deco et al., 2019). Briefly, we computed the distance between our model and the empirical grand average phase coherence matrices (as a measure of synchronization of the system) of the healthy controls group. In the stroke patients' group, we adjusted each structural connection separately using a greedy version of the gradient-descent approach. In order to work only positive values for the algorithm, all values are transformed into a mutual information measure (assuming Gaussianity). Therefore, the individual subject information is introduced by means of its disconnection (SC + each subject SDC) derived from the LQT. The equation of the optimization is as follows: (For more information, see Deco et al., 2019).

$$C_{ij} = C_{ij} + \varepsilon\left(FC_{ij}^{phases\_emp} - FC_{ij}^{phases\_mod}\right). \tag{5}$$

Where "C" is the anatomical connectivity and is updated with the difference between the grand-averaged phase coherence matrices (Empirical: $FC_{ij}^{phases\_emp}$ and model: $FC_{ij}^{phases\_mod}$, scaled by a factor $\varepsilon < 0.001$). The prediction, therefore, is based on the current estimation of the structural connectivity, which gets updated optimizing the phase FC in each iteration. In summary, the model was run repeatedly with recursive updates of EC until convergence was reached.

The distinction between functional and effective connectivity is crucial here: FC is defined as the statistical dependence between distant neurophysiological activities, whereas EC is defined as the influence one neural system exerts over another providing directionality in the relations making the matrices asymmetrical (Friston, 2011; Friston et al., 2003).

In the current study, we also added the structural disconnection masks (previously mentioned in this section) to the structural connectivity information provided by the simulations. Therefore, different models were used in the analysis (Fig. 1a). Only using the structural information (SC-based model), using the effective connectivity information (EC-based model), and lastly, using the effective connectivity information plus the structural disconnection mask information (EC with SDC mask model). For the last one, the optimization benefited from the information of the SDC when optimizing the model.

2.7. EC correlation with clinical and behavioral variables

Based on the work of (Favaretto et al., 2022), we tested whether the EC measures added some significant information to the obtained results from the static FC and dynamical FC combination in describing the behavioral outcome. We calculated the dynamical functional states (DFSs) using a sliding—window temporal correlation (window width = 60 s, window steps = 2 s) followed by eigenvector decomposition and clustering to establish the connectivity states that continuously activate across time. By construction, only one of the DFSs was active for each sliding window. The dynamic of the FC for each patient could be described in terms of a single time series of discrete values that alternates across time. In other words, a DFS is a spatial map of the edges between brain regions which shows consistent co-modulation in time

(Cabral et al., 2017b; Cabral et al., 2017a). Only a subset (n = 44) of the subjects was used for the DFSs analysis. The subset was made in order to use patients that were not employed for the principal components analysis. For more information, see (Favaretto et al., 2022). For each domain score, lesion volume, and total NIHSS score, we estimated the parameters of a Generalized Linear Model (GLM) with the Effective connectivity static principal components (SPCs) as the regressor and each behavioral score as output. We retained only SPCs which explained at least 5 % of the total variance, and that corresponded to an eigenvalue of the covariance matrix larger than 1, yielding to 2 SPCs. Therefore, for the regressor, we used the first two PCs (explaining 32 % and 12 % of the variance of the original data, respectively) adding to a total of 44 % of the variance explained. Then, we estimated the GLM with both SPCs from the EC and three dynamical PCs scores obtained from the above DFSs as regressors. The dynamical PCs scores capture numerous measures related to dynamical functional connectivity (Favaretto et al., 2022). It is relevant to clarify that the DFSs were added to the result of the models and were not computed every time.

The behavioral domains' assessment was described more in detail in the "Neuropsychological and behavioral assessment" section. We used all the regressors (static in combination with dynamic) at the acute stage to estimate the behavioral scores. No adjustments were necessary as the number of regressors was kept constant. In other words, as the comparison was made within the SPCs and within the SPCs + dyn PC, but not between them, the amount of regressors was the same in each comparison and therefore, not requiring any correction to solve the difference in their quantity of variables.

2.8. Classification procedure

Previous literature performed classification analysis by using EC, we tested how EC classification differs from other models using SC and FC as division criteria. The subjects were split into two equal groups by using the corresponding medians of SC lesion (number of damaged voxels in the lesion) and FC principal components. Therefore, our results could be compared with those of previous studies. The same procedure was performed with the principal components of two different models (EC and the EC + SDC mask) to end up with the four separation criteria (SC, FC, EC and EC + SDC). To achieve this classification, we used the neuropsychological scores to classify patients who were divided based on their median split, applying a random forest algorithm.

Briefly, the random forest algorithm builds upon the concept of a decision tree classifier, where samples are iteratively split into two branches depending on the values of their features (Breiman, 2001; Sanz Perl et al., 2021).

We trained and evaluated a random forest classifier to distinguish different levels of severity, estimated based on the neuropsychological test results. We used the neuropsychological scores (see "Neuropsychological and behavioral assessment") as features to classify using a random forest algorithm whether patients belonged to the low severity or high severity group based on the above criteria (SC, FC, EC, EC + SDC). Diving the dataset by using the median of:

1) The lesion volume obtained from the SC segmentation (from the lesion itself) indicating the number of voxels affected by the lesion.
2) The summation of the singular values of the first two PCs obtained from the FC information.
3) The summation of the singular values of the first two PCs obtained from the EC information.
4) The summation of the singular values of the first two PCs obtained from the EC information (with the SDC mask).

We trained random forest classifiers with 1000 decision trees using 80 % of the subjects through cross-validation analysis. Different training criteria were calculated and presented in Fig. S5. All accuracies were determined as the area under the receiver operating characteristic curve

(AUC) (For more information, see (Sanz Perl et al., 2021)).

2.9. Topological measurements

The directionality of EC opens the field to explore various topological attributes that cannot be done or are less informative in symmetrical and undirected networks such as the FC. In the current study we introduce a small group of these metrics:

1) Broadcasters' percentage was calculated as the mean of the number of successors (number of nodes forming directed edges from which the node is the source, without counting the reciprocal relations) divided by the amount of the neighbors (all the nodes connected, disregarding the directionality). A connection is labeled as reciprocal when the number of successors and receivers are the same, while a connection is directed when these values are not identical.

$$Broadcasters' \ percentage = \frac{Successors(excluding \ reciprocal \ relations)}{Amount \ of \ neighbors}$$

2) Receivers' percentages were obtained in the same way but with predecessors (number of nodes forming directed edges from which the node is the target, without counting the reciprocal relations) instead of successors.

$$Receivers' \ percentage = \frac{Predecessors(excluding \ reciprocal \ relations)}{Amount \ of \ neighbors}$$

3) Broadcasters' amount was calculated by counting how many nodes were having a higher weight of outgoing information than incoming and then average across patients.

$$Brodcasters' \ amount = \sum nodes, \ if \ Succesors > Predecessors$$

4) The receivers' amount was calculated by counting how many nodes were having a higher weight of incoming information than outgoing and then average across patients.

$$Receivers' \ amount = . \sum nodes, if Succesors < Predecessors$$

5) Reciprocity was calculated by obtaining the ratio between reciprocal connections and the total amount of neighbors of the corresponding node. Since the EC estimation procedure set some directional connections to zero, reciprocity is present in fewer connections than in FC calculations.

$$Reciprocity = \frac{Reciprocal \ relations}{Amount \ of \ neighbors}$$

6) Average path length was calculated as the mean distance of the nonzero values of the network. of the Effective Connectivity Matrix (ECM).

$$Distance \ matrix = \min(Distance(ECM))$$

7) Communicability was used to calculate the relation between different nodes by using the shortest path of the Effective Connectivity Matrix (ECM).

$$Communicability \ matrix = \frac{ECM - Min(ECM)}{\max(ECM) - \min(ECM)}$$

2.10. Lesion assessment based on region interaction

To analyze the interaction between brain regions, each patient's structural connectivity matrix was segmented into three different groups: The intersections connecting cortical nodes with other cortical nodes, cortical nodes with sub-cortical nodes, and finally subcortical nodes with other subcortical nodes. The association between each of three different groups and other variables of interest was inspected. For assessing the value of each group, three different approaches were used giving similar results. These approaches consisted of total disconnection (how many nodes were completely disconnected), partial disconnection (percentage of disconnection of nodes that were not completely disconnected), and the combination of both. As in the previous sections, the relationship between the variables was assessed without performing any type of prediction.

3. Results

We derived a whole brain model to infer the dynamical effects of stroke lesions two weeks after onset. We calculated four different models: Healthy control model (without EC) and Healthy control model (with EC) based on a healthy atlas structural connectome (see methods) in combination with individually measured fMRI BOLD signal. A variation of the second one was calculated for a posterior comparison using the stroke patients' fMRI BOLD signal instead of the previously mentioned healthy control fMRI BOLD signal (referred as SC-model). Stroke model with EC (referred as EC-Model) integrates the healthy connectome with each patient fMRI BOLD signal in order to use the resulting EC as input for the model. Lastly, the Stroke model with EC + SDC (referred as EC + SDC model) integrates the healthy connectome weighted in stroke patients by the structural disconnection produced by each individual lesion (one connectome per patient) next to each patient fMRI BOLD signal as input for the model. In contrast, one structural connectome was used for the healthy subjects as an average for the entire group based on the Yeo atlas (Yeo et al., 2011). To render the connectome directional, it was adjusted by the phase differences between regions computed on group average functional connectivity data. Then, we estimate the computational model based on coupled Stuart Landau oscillators (Fig. 1a). The presented model contains a global scale factor, also referred to as G coupling value, which assesses the influence of the SC in the model. We selected the optimal value in which the model phases were more like the empirical data. As the optimal model fit (simulated FC to empirical FC) is dependent on the global coupling, in the current study, we use the healthy control dataset to calculate this parameter. The result was a value of 3.1, as the most efficient for the used model, obtained by an exhaustive exploration of the homogeneous parameter space (a, G) around the Hopf bifurcation (a $\approx$0). It is important to clarify that the G value is a scaling factor of the SC, which was adjusted in the model through iterations for each subject.

We developed an effective connectivity (EC) model in healthy controls and adjusted it in stroke patients to account for different descriptions of the structural damage. EC captures directional interactions between regions of the brain. In the healthy control group, we computed the distance between the model and the empirical grand average phase coherence matrices obtained from the empirically measured fMRI signals. In stroke patients' group, we adjusted each structural connection separately using a greedy version of the gradient-descent approach. The resulting EC (Fig. 1a) reveals the influence of one region over another in a direct way and provides information on asymmetrical regional pairwise temporal interactions. The model fitting was assessed for each patient in order to represent the similarity between the simulated and the empirical data at the subject level (Fig. 1b).

By using a principal component analysis (PCA) of the resulting ECs, we calculated the relation between the main components and behavioral performance of the stroke patients (Fig. 1c). Furthermore, we classify the level of damage severity using a machine learning algorithm, revealing the enhanced performance compared to approaches used in previous studies. Finally, we calculated graph topological metrics in order to show how network dynamics change after a stroke injury.

The presented mechanistic generative whole-brain model reveals the
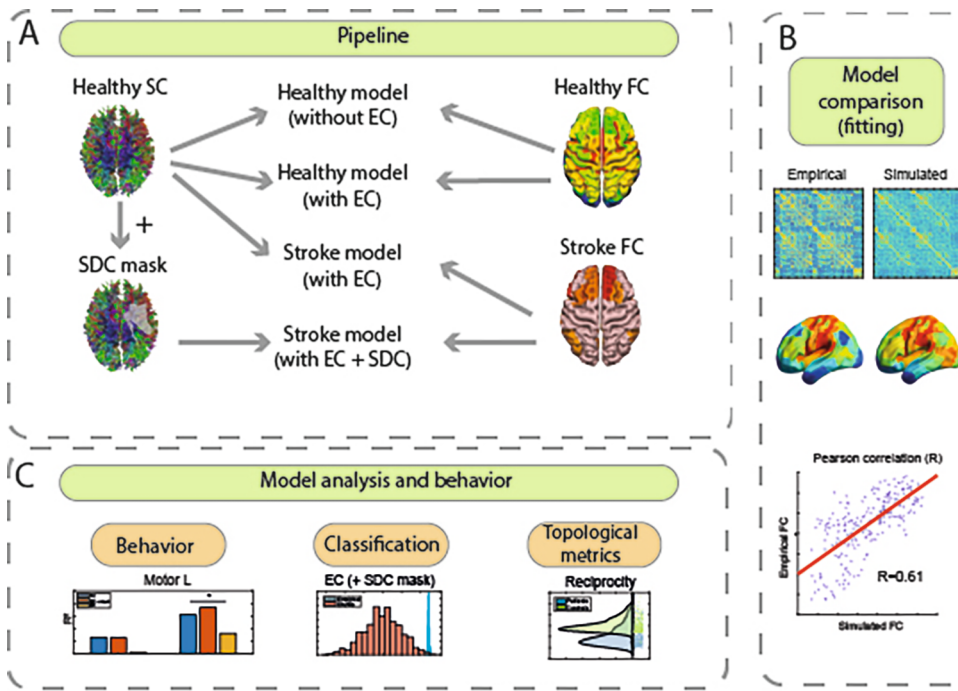
Fig. 1. Pipeline of methods used for the analysis. (A) Pipeline: Four different models were created: Healthy model without effective connectivity (EC) and Healthy model with EC, both composed of healthy controls SC and healthy controls FC; Stroke model with EC, composed of healthy controls SC and stroke patients FC; Stroke model with EC plus SDC mask, composed by Stroke patients SC (Healthy SC + SDC mask) and stroke patients FC. A variation of the second model (Healthy model with EC) was calculated as a comparison, later called as SC-Model where instead of the healthy controls FC, the stroke FC was used. The control parameters of all the models were tuned using the grand average FC derived from the healthy controls' fMRI BOLD data. For modeling local neural masses, it was used the normal form of a Hopf bifurcation. EC is calculated by optimizing the effectiveness of the synaptic connections between brain regions as specified by the SC. (B) Model comparison (fitting): The model fitting was assessed for each subject and the Pearson correlation was calculated to check the similarity between the empirical and the simulated. (C) Model analysis and behavior: To analyze the properties underlying the EC, we performed a Principal Component Analysis (PCA), with which results, we measure their associative strength with the neuropsychological assessment (behavior) and their sensitivity to classify the severity of the stroke in each patient. Furthermore, topological metrics were calculated taking advantage of the asymmetric feature of the EC.

consequences of the stroke lesions by benefiting from structural disconnection maps revealing the importance of the anatomical connectivity disruption at the subject level.

3.1. EC-based whole-brain models with disconnection masks reproduce FC impairments in stroke patients

In the first analysis, we intend to test how different whole brain models predict the most common FC abnormalities found in stroke patients, specifically: 1) a decrease of negative intra-hemispheric FC between regions of the Dorsal attention networks (DAN) and Default mode network (DMN); 2) a decrease of inter-hemispheric homotopic FC; 3) a decrease of modularity. We compared models that simulated FC or EC, each with different kinds of information: no lesion information, gray matter damage, and white matter SDC.

We first considered the Intra-hemispheric FC, i.e., the average pairwise correlation between regions of the DAN and DMN. We only considered the damaged hemisphere to avoid diminishing the effect with the preserved hemisphere. As in previous work (J. C. Griffis et al., 2019; Siegel et al., 2016), the empirical FC in healthy controls shows a negative correlation that is decreased (less negative) in stroke ($t(121) = -2.08$, $p = .03$). In contrast, the model FC, both without or with gray matter or SDC mask, is not significantly different between healthy and stroke ($t(121) = 0.2, p = .83$). However, the simulated EC, only when the SDC mask is applied, showed a significantly less negative correlation than controls, in agreement with the empirical data ($t(121) = -10.5, p < .01$) (Fig. 2a). It should be also noted that all FC and EC model measures have a much smaller variability than the empirical measures. This is due to the optimization of the model that used the same parameter value (G-coupling). Therefore, the only source of variability in the model for all the patients was the noise, losing variability information through the process.

Next, we consider the Interhemispheric FC measured in healthy and stroke patients. As in previous work, interhemispheric homotopic FC

was significantly stronger in healthy subjects than in stroke patients ($t(121) = 3.84$, $p < .01$). Using SC-based models there was no significant FC difference between groups ($t(121) = -1.09$, $p = .27$). Again, the EC-based model only when using the SDC mask replicated the normal pattern ($t(121) = 68.60$, $p < .01$)(Fig. 2b).

Thirdly, we consider modularity. In stroke, when considering a given functional parcellation, modularity is decreased and recovers over time (Siegel et al., 2018). This result was replicated: controls showed a significantly higher modularity value than patients (2 weeks post-stroke) ($t(121) = 2.98$, $p < .01$). Again, the FC models with or without masks failed to replicate the empirical pattern ($t(121) = 2.05$, $p = .06$), while EC models that included the SDC mask did replicate ($t(121) = 53.14$, $p < .01$)(Fig. 2c).

In Summary, this analysis shows that whole brain EC models that include structural disconnection information resemble the empirically observed FC abnormalities in stroke patients including intra-hemispheric, inter-hemispheric, and modularity. Other models that do not include lesion information or only gray matter damage, do not resemble empirical results.

3.2. EC-based whole-brain models show the best fitting to the empirical data when including structural disconnection information

Next, in order to inspect the validity of the models, we checked how the different models fit the empirical data. Therefore, we assessed the quantitative similarity between empirical FC and simulated FC from different models (SC, EC, and EC with SDC mask) in stroke patients.

The EC-based model with SDC masks showed the highest correlation with the empirical data (mean = 0.52), next the EC-based model without SDC masks (mean = 0.32), last the SC-based model (mean = 0.27). Fig. 3a displays the topology of the empirical and simulated FC. Fig. 3b reveals the group analysis of this phenomenon including the correlation by node of one example subject (bottom). This result shows the validity of the presented model and the importance of the SDC mask. The same
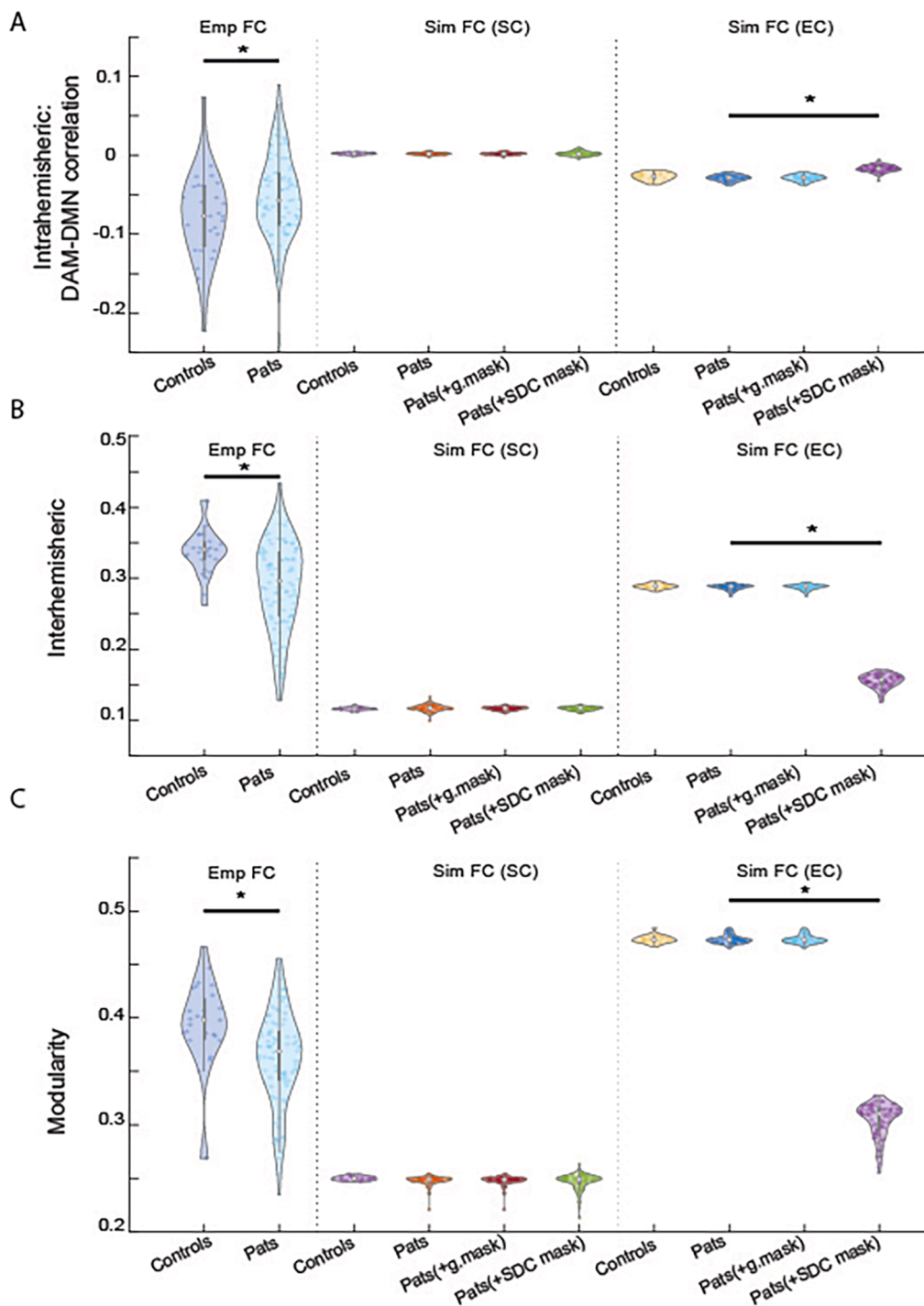
Fig. 2. FC impairment in stroke and replication with whole-brain mechanistic model: Comparison between patients and controls in their empirical FC (left), SC-based model (center), and EC-based model (right) in (A) intrahemispheric value, (B) interhemispheric value, and (C) modularity value. Both models are performed with and without mask including the comparisons between the SDC mask and the gray matter mask (See Methods). The model based on EC showed to be more like the empirical FC (compared to the model based on SC) due to it was trained to optimally fit the empirical data.

analysis was run on the control group model showing that the level of correlation in healthy controls is similar to that obtained in stroke patients (Fig. S9).

In summary, this analysis shows that whole brain models that include SDC information have the highest resemblance to the empirical data showing the value of the lesion information in the presented models.

3.3. EC-based whole-brain models show abnormalities of network communication in stroke

Having established that EC-based whole brain models replicate the most common FC abnormalities in stroke, and that are the most accurate in replicating empirically measured FC, it is now possible to examine deficits in communication, specifically differences in directional interactions both within stroke patients and between stroke and controls.

Hence, we compared within and between network communication of EC in both patients and controls (Fig. 4A). The sum of weights of the connections was Fisher z-transformed to show the difference. The matrix is organized with sender nodes on the vertical axis and receiving nodes on the horizontal axis.

In controls there are strong within-network and inter-hemispheric homotopic interactions. There are also strong interactions between networks. It is apparent that the DMN is the strongest sender (left: [*F*
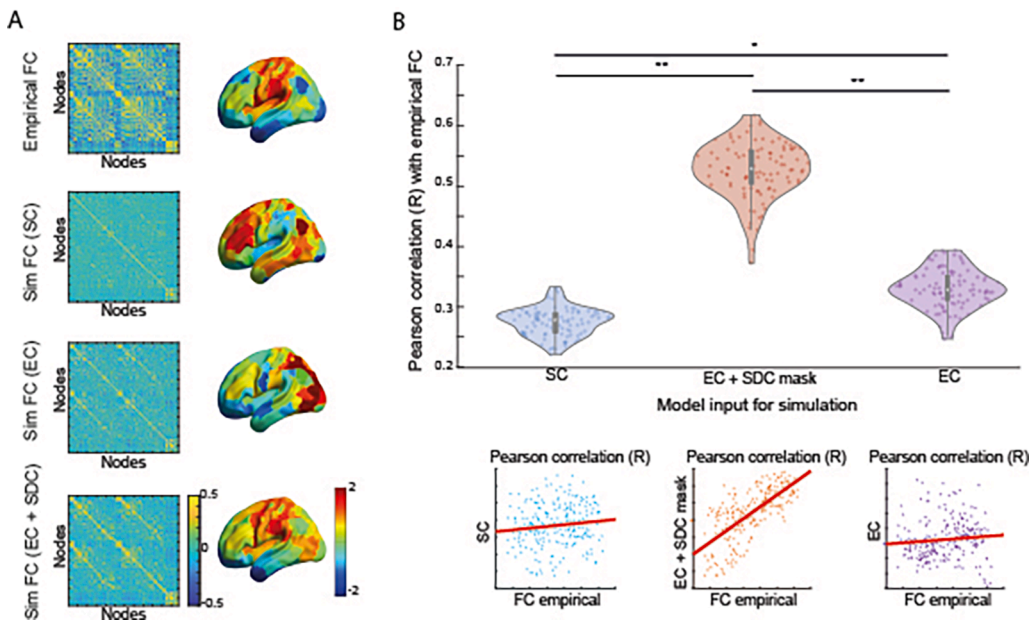
Fig. 3. Model similarity: (A) FC matrices for empirical data (top), Simulated FC using SC (center-top), Simulated FC using EC (center-bottom) and Simulated FC using EC plus the SDC mask (bottom). Matrices were illustrated in brain surfaces to help visualization revealing the topological localization of the effects. (B) The correlation between the empirical data and each of the aforementioned models. The highest correlation was observed in the model based on EC plus SDC masks. Group results are displayed (top) while also individual result from one example subject is shown (bottom).
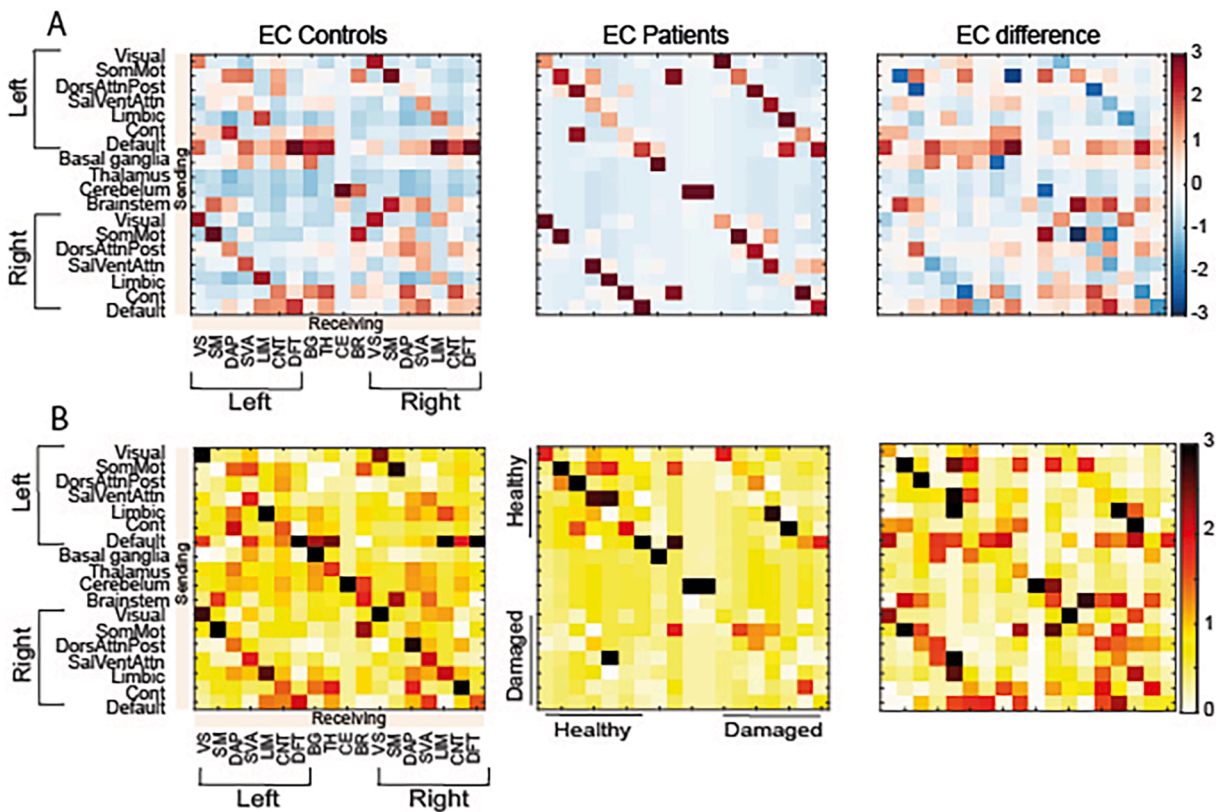
Fig. 4. Networks interactions: (A) Network interactions for the EC of (left) controls, (center) patients. The right panel exposes the difference for each interaction between the two groups. (B) Network communication comparing damaged from healthy hemisphere: In center and right panels, the matrices were re-organized to have all the damage hemispheres together on one side and all the healthy hemisphere on the other.

$(6,119) = 7.78, p < .01$; mean $= 1.28$, SD $= 1.25$; right hemisphere: $([F(6, 119) = 2.73, p = .01]$; mean $= 0.53$, SD $= 0.77)$. DMN therefore appears to be the network with the strongest influence on other networks (See discussion).

Stroke patients seem to maintain robust within-network homotopic interactions, but much weakened between-network interactions. This can be observed clearly in the difference matrix in Fig. 4A (EC

difference). Statistical comparisons among networks are shown in Fig. S8 with the strongest differences in DMN, somatomotor, brainstem, and basal ganglia.

However, more information emerges when all lesions are flipped to one side and then comparing healthy to damaged hemisphere (Fig. 4B). These matrices indicate that regions in the damaged hemisphere do not 'send' to homotopic healthy hemisphere regions, while such influence is

maintained in the opposite direction from healthy to damaged hemisphere (compare off-diagonal interaction for healthy (upper) and damaged (lower) hemisphere networks). Between networks interactions seem to be damaged in both healthy and damaged hemispheres.

In summary, the EC models show interesting impairments in communication from the lesioned to the healthy hemisphere, and a loss of interaction between networks which is especially evident in the DMN and a few other networks. This approach will be discussed in relation to other methods to study interactions, e.g., Granger causality.
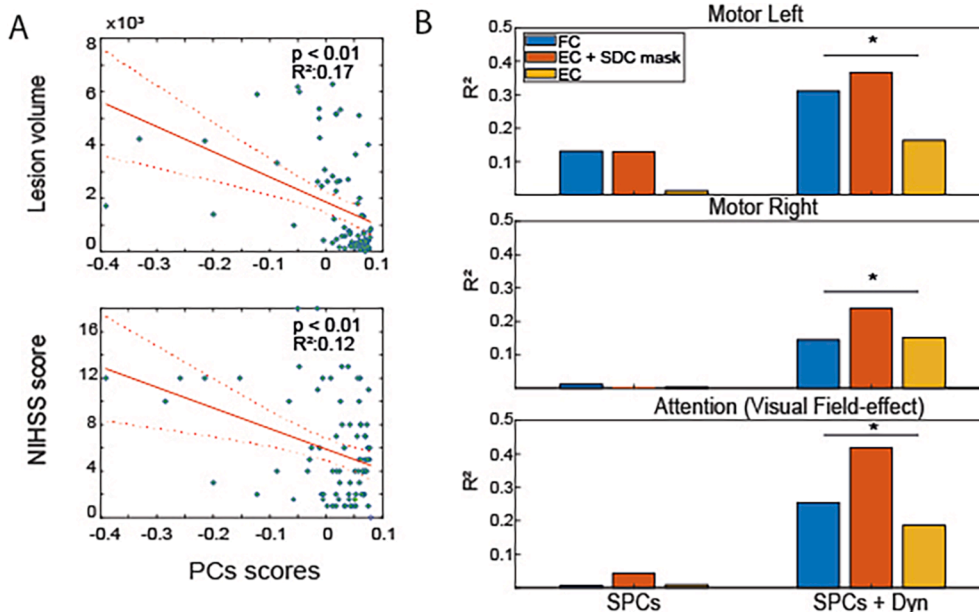
3.4. EC-based whole-brain models and correlation with clinical variables

In the next analysis, we explored the correlation between (simulated FC from) EC-based models and lesion, clinical, and behavioral variables. The analysis aims to shed light on the relation between lesion metrics (such as lesion volume and NIHSS score) and behavioral variables (such as motor tasks). Furthermore, we compared the obtained outcome with previously reported results in order to show the robustness of the presented models.

To reduce the spatial variability across all brain regions, we first computed the PCs (calculated as the singular value of the first two principal components) from the EC model. Two static PCs explained 44 % of the total variance (see methods) and explained a significant percentage of the lesion volume variability ($R^2 = 0.17$, $p < .01$), and clinical severity based on the NIHSS score ($R^2 = 0.12$, $p < .01$) (Fig. 5a).

Next, we explored how these PCs were related to behavioral deficits using a subset of patients from (Favaretto et al., 2022), in contrast to the complete set used in the previous analysis. Here we considered both static components (computed on the time-averaged data) or dynamic components based on a state decomposition analysis (see Methods) (Favaretto et al., 2022). It is important to clarify that the comparison was made only with the subjects for which we obtained the SPCs and Dynamic PCS.

The EC static principal components (SPCs) did not show any significant association with behavior (Fig. 5b). However, the behavioral association in some domains improved when static and dynamic EC components were combined: Motor-Left ($R^2 = 0.36$, $p < .01$), Motor-Right ($R^2 = 0.23$, $p = .05$) and Attention Visual Field-effect (AttentionVF) ($R^2 = 0.41$, $p < .01$). In all domains, except for Attention validity/Disengagement, PCs from EC associative value were higher when performed with the damage mask (Sup Fig. 3).
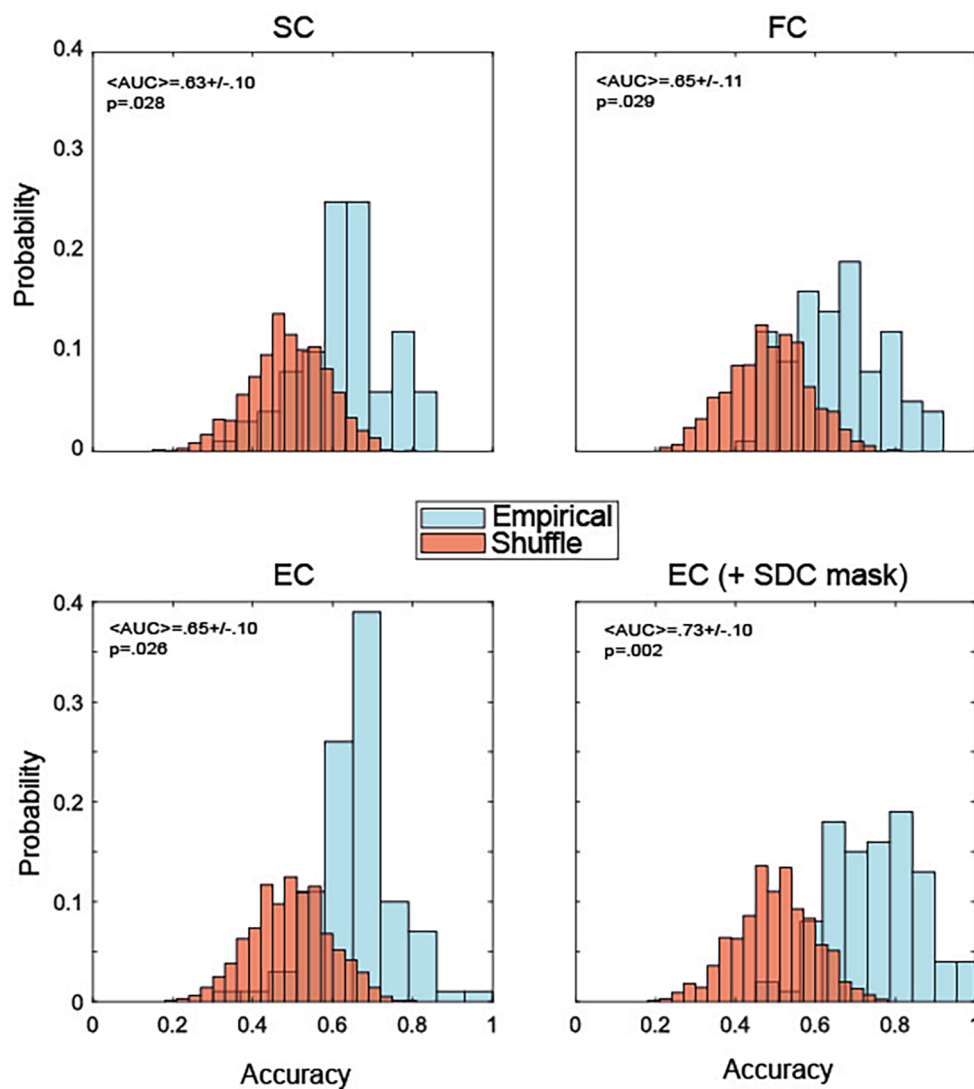
In summary, not only the PCs from the EC model were related to lesion metrics but also outperformed previously reported metrics in existing literature, in their relation to clinical variables such as behavioral impairment.

3.5. EC-based whole-brain models and classification of behavioral impairment

In the next analysis, we intend to test the utility of the whole brain models for the classification of patients' lesion severity in order to contribute to their diagnosis. Hence, we implemented a classification algorithm in order to distinguish patients' lesion severity using as input the results of the behavioral tests. The division of patients according to their structural disconnection was based on the median value of their lesion volume, separating the sample into two equal groups.

Given the heterogeneity in lesion location and behavioral deficits across patients, we infer that FC dynamics would be differently affected depending on the severity of the static FC impairment. Therefore, we applied a Principal Component Analysis (PCA) to the static FC of acute patients (after z-scoring to the average FC of control subjects) to split into a low and high severity group. Then, we used the same logic to divide the sample using the PCs of the previously mentioned models. As a result, the prediction of behavioral impairment is based on a median split of the subjects' singular value (Derived from PCA analysis) according to different criteria (SC, FC, EC, EC with SDC mask). By using a random forest classifier, we obtained the area under the curve (AUC) representing the accuracy of the classifier for high severity injury patients and low severity injury values, according to the median score. We used the performance in the neuropsychological tests, including all the behavioral domains (explained in the methods section), of the patients to test the algorithm and assess the classification. The scores were z-scored to get one score across domains. The outcome is visualized as histograms (Fig. 6). Each row represents classification based on different signals (SC, FC, EC, EC with SDC mask). The histograms in blue correspond to the AUC values obtained using the real data, while the histograms in red indicate the AUC values obtained after shuffling the data labels. Label shuffled is used as a null model to obtain the p-values shown in the insets.

To measure the statistical significance of the accuracy values, we trained and evaluated a total of 1000 classifiers using the behavioral scores of the patients but scrambling the class labels. Afterward, we

Fig. 5. Association strength of EC and enhancement by using SDC mask: (A) Relation between the values obtained from the PCA of the EC and (top) the lesion volume (Calculated in voxels amount from the SC), and (bottom) the NIHSS score. (B) Associative strength of three behavioral domains given by the static PCA (SPCs) of the three approaches (FC, EC with the SDC mask and EC without the SDC mask) and with their corresponding interaction with the dynamical components (see Methods for details). Asterisk indicates when only one regressor shows a significant relationship between the three measurements.

Fig. 6. Improving classification of severity level by using EC: (A) Each plot represents a different criterion of classification of the two groups. Histograms of AUC values for the random forest classifiers trained to distinguish low from high severity behavior impairment using as division criteria: the lesion volume of the SC (top-left), the PCs of the FC (top-right), the PCS of the EC (bottom left) and the PCs of the EC with the SDC mask applied (bottom-right). All classifiers were tested using the neuropsychological assessment performances. Histograms in blue correspond to data without label shuffling, while red indicates AUC after label shuffling. (For interpretation of the references to color in this figure legend, the reader is referred to the web version of this article.)

produced an empirical p-value by counting how many times the accuracy of the classifier with scrambled class labels was greater than that of the original classifier. All accuracies were determined as the area under the receiver operating characteristic curve (AUC). The EC (with SDC mask) showed the highest performance (mean = 0.73, SD < 0.10, p <.01) followed by EC (mean = 0.65, SD < 0.1, p =.26), FC (mean = 0.65, SD < 0.11, p =.029) and SC (mean = 0.63, SD < 0.10, p =.028) (Fig. 6). Same information is summarized in Sup. Table. 1. The presented result is obtained by using 80 % of the subjects during the training of the cross-validation classification. For an exploration of other ratios of training, see Fig. S5.

In summary, the highest performance to classify behavioral impairment was obtained by using the EC-model including the disconnection information, showing another contribution of the presented models for stroke patients' diagnosis.

### 3.6. Topological measures in EC-based models

Since the EC represents the directed non-symmetrical interactions between brain regions, it is possible through graph metrics to describe differences in the topological organization between healthy controls and stroke patients by means of a group level analysis. Following that line, the next analysis will explore a diverse range of graph metrics in order to show how they reflect the difference between the two groups.

In the comparison between stroke patients and healthy subjects, patients have a significantly higher degree ratio per node, both in broadcasters ($t(121) = 113.04$, p <.01), and in receivers ($t(121) = 123.16$,p <.01). Moreover, when comparing broadcasters to receivers, all patients had a larger number of broadcasters than receivers (Fig. 7a). It should be noted that the difference in Fig. 7 with healthy controls is somehow exaggerated by the fact that all reciprocal connections were excluded for the calculation of broadcasting and integration. Metrics calculations are explained in detail in the Methods section.

In addition, the average path length was higher in patients than in the control group ($t(121) = 28.5$,p <.01), while the effect was the opposite for reciprocity and communicability where controls showed significantly higher values than patients ($t(121) = -14.59$, p <.01 and $t(121) = -41.13$, p <.01 respectively).

To examine the influence of lesions on these metrics, the damaged hemispheres were aligned on the same side. Broadcasters' percentage was higher in the healthy hemisphere compared to the damaged one ($t(190) = 67.01$, p <.01)). The same effect was visible in the reciprocity level ($t(190) = 31.54$, p <.01)), while the reverse direction was observed in the receivers' percentage ($t(190) = -49.09$, p <.01)) where higher values occurred in the damaged hemisphere (Fig. 7b).

These findings suggest that communication is less efficient in stroke patients (longer path length, lower reciprocity, and communicability), and this depends on a topological organization in which the integration
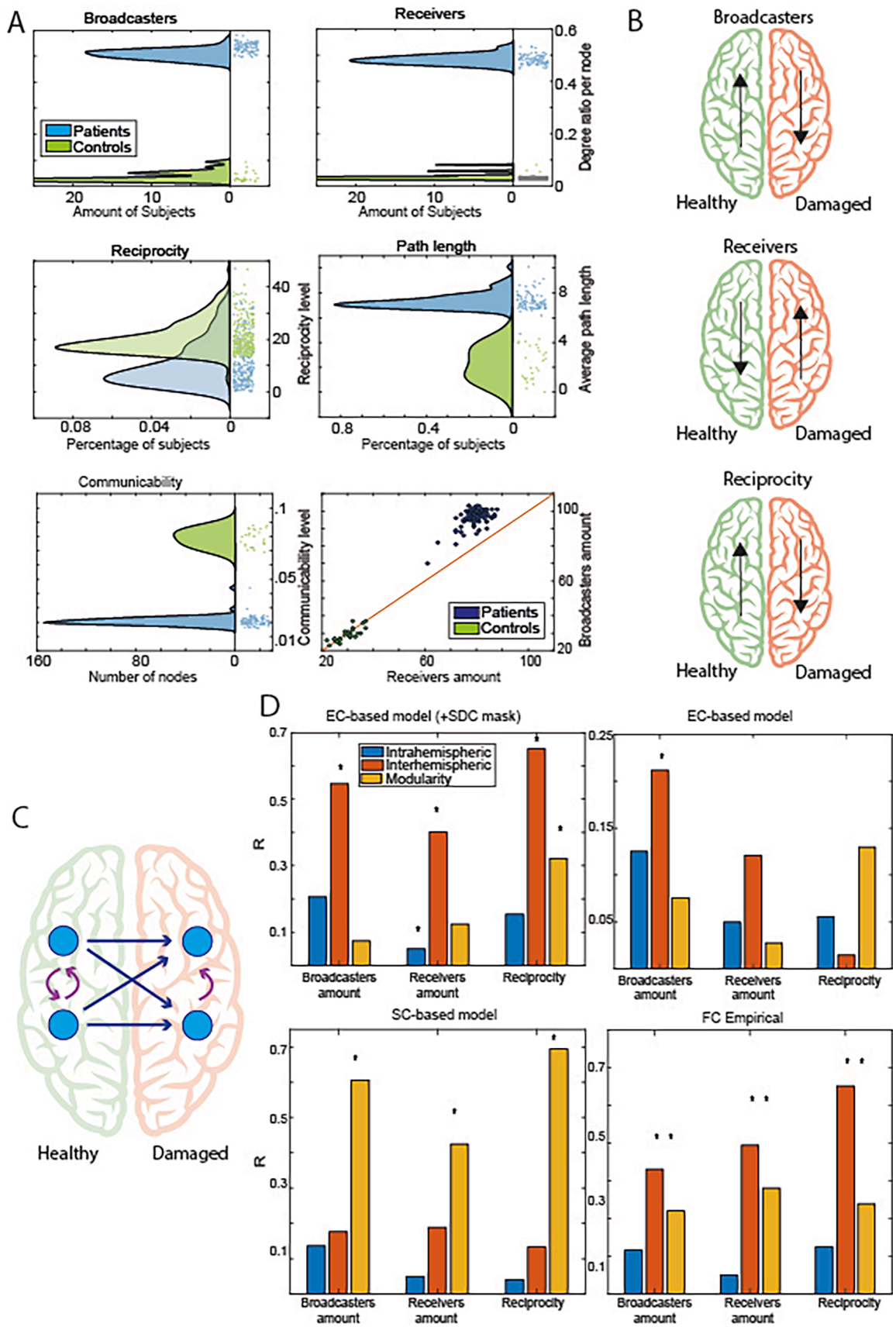
(caption on next page)

Fig. 7. Topological measures benefited from EC: (A) Comparison between stroke patients and healthy controls in (top-left) the amount of broadcasters per node, (top-right) the amount of receivers per node, (center-left) reciprocity per node, (center-right) average path length and (bottom-left) communicability. At the bottom-right graph, it is visible the relation between both the number of receivers and broadcasters in both sample groups. (B) Hemispheres were flipped when corresponding to align the damaged and healthy hemispheres. Differences in ratio of Broadcasters (top), receivers (center) and reciprocity (bottom) are represented with arrows. (C) Visualization of connections in both healthy and damaged hemisphere indicating the relevance of interhemispheric communication. Blue arrows show the broadcasting increase in the healthy hemisphere and the receivers increase in the damaged hemisphere. Purple arrows indicate the superior reciprocity in the healthy hemisphere compared to the damaged one. (D) Relation between the FC impairments in stroke (Intrahemishperic, interhemispheric, and modularity) and the topological metrics of the EC (Broadcasters, receivers, and reciprocity) in (top-left) EC model with SDC mask, (top-right) EC model without SDC mask, (bottom-left) SC model, (bottom-right) empirical FC. (For interpretation of the references to color in this figure legend, the reader is referred to the web version of this article.)

among regions is abnormally high (higher broadcasters and receivers). Interestingly, this overall topological organization reflects an asymmetry between the damaged and healthy hemisphere, where the latter sends abnormally more to the damaged one.

Next, it is interesting to ask how this topological organization relates to the canonical FC abnormalities reported in previous work (Baldassarre et al., 2016; J. C. Griffis et al., 2019; Siegel et al., 2016). Hence, the relation between FC impairments in stroke (intrahemishperic, interhemispheric, and modularity) and the topological metrics of the EC (Broadcasters' amount, receivers' amount, and reciprocity) were investigated giving as a result 9 combinations (3 FC × 3 topological) (Fig. 7d). Using the empirical FC, 6 out of 9 correlations were significant, using the simulated FC from the EC model with SDC masks 5 out of 9 correlations were significant, while using the EC model without any mask, only one correlation was significant.

Interestingly all topological measures (broadcasters, receivers, and reciprocity) correlated significantly with the strength of interhemispheric FC and modularity, much less with intra-hemispheric FC. The model that includes only SC correlated significantly with the modularity, and since it did not contain any directional information, did not correlate with broadcasters or receivers.

There was a significant difference between patients with cortical lesions when compared with those with subcortical lesions: cortically damaged patients showed a lower value of broadcaster amount ($t(54) = -2.5$, $p = .013$), a lower value of receivers' amount ($t(54) = -2.42$, $p = .018$) and a higher value of path length ($t(54) = 2.28$, $p = .026$) (Fig. S6). This result implies that the topological measures capture prevalently cortico-cortical communication and less subcortical-cortical communication.

Conversely, we did not find any significant differences when comparing the patients with lesions in the left hemisphere and the right one ($t(94) = -0.5$, $p = .6$). Left and right hemisphere lesion produced topological measures that were strongly correlated: Broadcaster percentage: $r = 0.98$, $p < .01$; Receivers percentage: $r = 0.98$, $p < .01$; Reciprocity degree: $r = 0.92$, $p < .01$. This result implies that lesions on either side produce bilateral effects that are similar irrespective of the

side of the lesion.

In summary, topological differences between stroke patients and healthy controls can be obtained by the means of graph metrics, indicating how brain dynamics are modified due to the stroke incidents. Those differences got enhanced when the healthy and damaged hemispheres got aligned across all stroke patients.
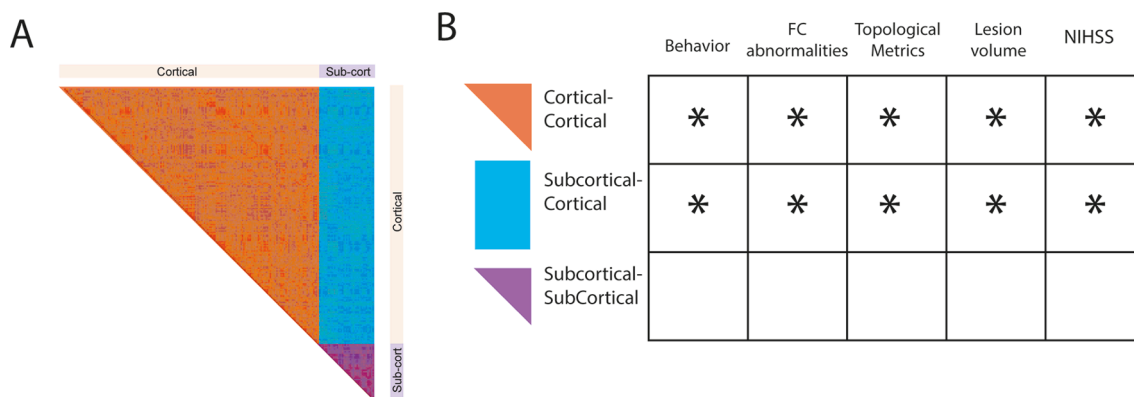
3.7. Relation between regions interaction and stroke-related metrics

For the final analysis, we explored the nodes' communication by inspecting the areas they are communicated to. Therefore, the edges of the corresponding nodes can be distinguished into different groups in order to observe which interactions are most associated with previous studied metrics. In order to localize which regions were involved in the affected nodes, we labeled the nodes based on which areas were being communicated. Each patient structural connectivity matrix was segmented into three different groups, edges that communicate two nodes from Cortical-Cortical (CC), nodes from Subcortical-Cortical (SC), and nodes from Subcortical-Subcortical (SS) (Fig. 8a). We performed correlations between the amount of lesion of each group and previously reported metrics. The relations between them are presented here (Fig. 8b).

Relation with behavior:

- There was a significant association between the CC group with Language ($r^2 = 0.36$, $p < .01$), MotorL ($r^2 = 0.10$, $p < .01$), MemoryS ($r^2 = 0.11$, $p < .01$) and Motor IC T1 ($r^2 = 0.10$, $p < .01$) while no significant relation with the remaining behavioral domains ($p > .1$)
- There was a significant association between the SC group with Language ($r^2 = 0.16$, $p < .01$), MotorL ($r^2 = 0.33$, $p < .01$), MemoryS ($r^2 = 0.20$, $p < .01$) and Motor IC T1 ($r^2 = 0.35$, $p < .01$) while no significant relation with the remaining behavioral domains ($p > .1$)
- There was no significant association between the SS group with any of the behavioral domains ($p > .2$)

Relation with FC abnormalities.

Fig. 8. Lesion volume classified according to region interaction and their relation with stroke-related metrics: (A) Distinction between three different types of lesions regarding the involved regions, Cortical-Cortical, Subcortical-Cortical and Subcortical-Subcortical. Color is used as a reference to distinguish the three different groups in a visual way. (B) Association between the lesion classification and behavior domains, FC abnormalities, topological metrics, lesion volume, and NIHSS. It is important to note that the lower amount of nodes in the SS group is influencing the reported results.

- There was a significant association between the CC group and interhemispheric level ($r^2 = 0.23$, $p <.01$) and modularity ($r^2 = 0.07$, $p <.01$) while there was no significant difference with intrahemispheric level ($r^2 = 0.01$, $p =.19$)
- There was a significant association between the SC group and interhemispheric level ($r^2 = 0.33$, $p <.01$) and modularity ($r^2 = 0.14$, $p <.01$) while there was no significant difference with intrahemispheric level ($r^2 = 0.001$, $p =.38$)
- There was no significant association between the SS group and any of the three FC abnormalities ($p >.1$)

Relation with Topological metrics:

- There was a significant association between the CC group and the number of broadcasters ($r^2 = 0.20$, $p <.01$), number of integrators ($r^2 = 0.33$, $p <.01$), and reciprocity level ($r^2 = 0.26$, $p <.01$)
- There was a significant association between the SC group and the number of broadcasters ($r^2 = 0.22$, $p <.01$), number of receivers ($r^2 = 0.19$, $p <.01$), and reciprocity level ($r^2 = 0.37$, $p <.01$)
- There was no significant association between the SS group and any of the topological metrics ($p >.3$)

Relation with Lesion volume:

- There was a significant association between the CC group and lesion volume ($r^2 = 0.72$, $p <.01$).

- There was a significant association between the SC group and lesion volume ($r^2 = 0.51$, $p <.01$).

- There was no significant association between the SC group and lesion volume ($r^2 = 0.01$, $p =.8$)

Relation with NIHSS:

- There was a significant association between the CC group and NIHSS ($r^2 = 0.10$, $p <.01$).

- There was a significant association between the SC group and NIHSS ($r^2 = 0.51$, $p <.01$).

- There was no significant association between the SC group and NIHSS ($r^2 = 0.01$, $p =.9$)

In summary, this analysis shows that region interaction in the structural disconnection information is related to previously reported metrics across this study. This provides an extra benefit for the inclusion of this information into the whole-brain models.

4. Discussion

In the current study, we created a generative model based on effective connectivity (EC) as a mechanistic answer to calculate post-stroke effects. The model replicates the most common FC impairments observed in previous literature by making use of the white matter structural disconnection caused by each patient's lesion (SDC mask). The EC model proves to be more strongly associated than previous models when relating to subjects' behavioral performance. More importantly, we demonstrate that the EC shows a higher performance when classifying the severity of the lesion. Finally, due to its asymmetrical property, it provides topological metrics useful for further analysis. All the presented methods and results contribute to shed light on the brain dynamics after stroke incidents, including the relevance of the structural disconnection information.

4.1. FC impairment in stroke

As reported in previous literature, there is a visible pattern of alterations in the FC of patients after stroke. These include an increase in the correlation of the intrahemispheric level (bringing it closer to zero), a decrease in the interhemispheric level, and a decrease in the modularity level (Arnemann et al., 2015; Baldassarre et al., 2016; Gratton et al., 2012; Siegel et al., 2016). While many studies focus on the concepts of integration and segregation (Adhikari et al., 2017; Bullmore & Sporns, 2009; Deco et al., 2015; Park & Friston, 2013; Sporns, 2013), their reduction poststroke could be the result of a single disruptive process such as the previously observed reductions in network modularity in the brain (Gratton et al., 2012). Moreover, modularity could be considered as a quantification of the ability of the brain to differentiate into separable subnetworks and is an essential property found in many complex systems that allows the system to develop dynamic behaviors (Meunier et al., 2010).

By using simulated models, the Hopf model that included only the SC information did not accurately replicate the empirical FC abnormalities (Fig. 3), while the model optimized with EC did, but only when the SDC mask was added. Notably, the model replicated the empirical FC effects only when the degree of white matter disconnection was taken into account, not the gray matter (parcel) damage as in (Adhikari et al., 2017). This illustrates the critical importance of white matter damage not only for understanding the physiological effects of stroke (Corbetta et al., 2015; Joseph C Griffis et al., 2019a; Griffis et al., 2020), but also for accurate modeling and prediction as illustrated in this work.

The current study underlines the validity of whole-brain computational models by complementing previous results (Joseph C Griffis et al., 2019a) with the information of SDC masks. The inclusion of the SDC masks should be taken into consideration in the future when modeling data of stroke patients.

Regarding the lesion localization, a clear distinction between cortical and subcortical patients is found when the SDC mask was included in the model, providing another advantage in using the presented model as a tool for future studies concerned about lesion localization and diagnostics.

4.2. Associative value of EC and enhancement by using SDC mask

Previous literature suggests that the relationship between the structural disconnection and the functional connectivity patterns (FC) should be low-dimensional (Corbetta et al., 2015; Joseph C Griffis et al., 2019a) as the components which explained most of the variance could provide useful information about cognitive and behavioral impairment (Bayrak et al., 2019).

In comparison to a recent study (Favaretto et al., 2022) that focused on the influence of the FC components and their interaction with dynamical features, this study aims to prove the enhanced associative value of the EC components.

We investigated the associative power over all the described domains (Fig. S3). By comparing the dynamical components combined with the PC provided by the FC and EC, the latest showed higher accuracy, especially for motor deficits. This is consistent with previous literature which claimed that functional alterations of brain networks are important for cognitive functions that rely on distributed networks (e.g., memory, attention, language), as compared to visual and motor functions for which structural damage is more sensitive (Corbetta et al., 2018). By performing a model which includes structural information, the relation over domains more sensitive to structural damage was more likely to get enhanced. It is important to underline that the present model combines both structural and functional information, providing more information compared to the analysis using only functional data (Favaretto et al., 2022). Future studies could introduce alternative models to control this issue.

4.3. Network communication reveals loss of interaction after stroke

Several studies have discussed the role of DMN as a brain hub (Power et al., 2013; van den Heuvel & Sporns, 2013). Here we found that the DMN is the network that exerts the main influence over other networks and that this influence is significantly decreased in stroke patients, both in the damaged and healthy hemisphere. A functional-anatomical gradient of cortical organization going from sensory-motor networks to polymodal tertiary association networks, with the DMN sitting at the top of this hierarchy has been described (Margulies et al., 2016), situating the default-mode network along a principal gradient of macroscale cortical organization (Raut et al., 2020). Hierarchical dynamics as a macroscopic organizing principle of the human brain (Mitra & Raichle, 2016) and human cortical–hippocampal dialogue in wake and slow-wave sleep (Mitra et al., 2016) have also been described. This organization is exactly the one mandated by hierarchical generative models. Networks that occupy higher levels may continuously generate predictions to suppress prediction errors of lower brain networks, such as primary sensory and motor regions, which may be engaged when prediction errors cannot be readily canceled out. The role of the DMN in exerting influence on other networks as shown here is consistent with this interpretation, and further suggests the testable hypothesis that stroke patients' deficits may partly reflect prediction errors in sensory-motor-cognitive processing.

This analysis also provides converging evidence on the alterations of directional interactions caused by focal stroke lesions. Allegra et al. (Allegra et al., 2021) measuring Granger causality (GC) on BOLD time-series found that focal lesions cause a relative decrease of GC from the damaged to the healthy hemisphere, as well as a decrease of interactions within the damaged hemisphere. Our results using EC-based models converge on this empirical observation similarly showing a loss of 'sender' influence from the damaged to the normal hemisphere, as well as an overall decrease of interactions within the damaged one.

4.4. Improving classification of behavior severity level by using EC

Previous studies (J. C. Griffis et al., 2019; Griffis et al., 2020; Wodeyar et al., 2020) showed, considering BOLD signals both at the voxel scale and ROI scale, that differences in structural connectivity were linked to changes in functional connectivity. Thus, found that, in the brain, communication between different regions is mediated through anatomical connections. The damaging effects perceived in stroke patients' FC were evident when also inspecting their SC, but not evident when looking at FC only.

Furthermore, the EC is calculated through simulations and modeling taking into consideration the anatomically restrained connections. In this study, the SC information was enhanced by the addition of the SDC mask. The classification using the EC information when applying the SDC mask showed the highest accuracy of classification, followed by a similar value by the EC without the SDC mask and afterward, with lower levels, the classification using only SC or FC. Despite providing a beneficial factor due to its enhanced classification power, further research is needed to know how this fluctuates across time and how the recovery of the patient is reflected in it.

The reported results by analyzing the z-abnormalities help to shed light on the relation between FC and SC. The generative model presented in the current study exposed how the effect changes in FC as a consequence of the stroke damage could be observed when the disconnection information is added. Nevertheless, in the damaged area and lesion severity classification, the direction of the effect was reversed between the empirical and the simulated data. Future studies could clarify the underlying reason for this discrepancy.

4.5. Topological measures benefited from EC

Previous studies discussed the role of graph theory metrics in stroke

patients (Han et al., 2020; Idesis et al., 2022; Sun et al., 2021; Vecchio et al., 2019b) revealing how properties such as global efficiency indicate the efficiency of integration of distributed information through the whole network. Nevertheless, the studies relied on FC to calculate the corresponding metrics. In the current study, the analysis profited from the asymmetricity of the EC to calculate topological metrics that could better describe the difference between stroke patients and healthy subjects. The calculation of broadcasts and receivers, used in the current study, excludes the relations that are spared reciprocally (both directions with a different node). Excluding the reciprocal relations (which are the majority), the higher number of broadcasters and receivers in the patients (compared to the healthy controls where an even higher percentage of the connections were reciprocal) was expected. The fact that every single patient presented a higher number of broadcasters than receivers is a relevant and unexpected result. Previous authors discussed this as an implication of a loss of integration converting it into a good biomarker for stroke treatment (Adhikari et al., 2020; Pallarés et al., 2018). Furthermore, a previous study (Chen et al., 2021) tried to manipulate this phenomenon through transcranial alternating current stimulation (tACS) exposing the difference in integration capacity in stroke patients. As reciprocity was found higher in controls, this metric could be used as a biomarker of patients' recovery. By assessing the reciprocity across time of each patient, it could be observed if the networks tend to partially restore, or at least compensate for, the deficit provoked by the damage.

While the distinction between patients according to the hemisphere damage did not reveal any significant information, the comparison between patients with cortical and subcortical lesions showed significant differences (when the corresponding SDC mask was applied) revealing that the measures explained could provide a novel method to assess distinctions in lesion localization.

The provided results open the possibility of using the metrics obtained in the current study to enhance the classification algorithms and create an even more accurate diagnosis.

4.6. Region interaction association with stroke metrics

Previous studies have reported the effects of after-stroke disconnections and their relation with global dynamic metrics such as modularity (Joseph C Griffis et al., 2019a; Warren et al., 2014). In this study, we divided the disconnection matrix of each patient into different groups relative to which regions' communication was impaired. We found a strong relationship between all the variables of interest and the Cortical-Cortical and Subcortical-Cortical groups while no association with the Subcortical-Subcortical group. These results support previous findings showing that stroke effects primarily disrupt whole-brain resting physiology by damaging interregional structural connections rather than only specific grey matter structures (Joseph C Griffis et al., 2019b). Based on these results, further studies could benefit from this approach to achieve more accurate analysis and reduce the amount of data used.

5. Limitations

The current study focuses on providing information about thr relationship with behavioral scores, classification of the severity of the injury, and providing informative topological metrics to analyze the brain dynamics properties. Nevertheless, it is not clear how these parameters are modified through the process of the recovery of the patients. Future studies could benefit from this longitudinal dataset in order to address these types of questions. Localization of the top 5 % weights in controls and patients is presented in Fig. S7 to allow comparisons in future studies which focus on the recovery after stroke. Furthermore, the dataset consisted of mostly ischemic patients and should be replicated in hemorrhagic stroke before being generalized to all the patients who suffered from a stroke.

Lastly, as beneficial as it was found, the EC consists of a bidirectional matrix instead of the typical symmetrical matrices obtained by analyses of FC and SC. Therefore, computational processes may be more time demanding and computationally costly.

6. Conclusion

The current study illustrated how the application of generative models provided a mechanistic explanation of the stroke effects in patients. We presented an approach to combine structural and functional data from stroke patients. The proposed model can also be used to compare different existing SDC masks to determine the one that produces the best fit to empirically observed FC. Together with the relevance of the SDC mask for the whole-brain models of stroke, the current study replicates the existing biomarkers of stroke damage and provides evidence that the proposed model can improve the classification accuracy of behavioral deficits after stroke. The present study opens a vast number of possibilities for further analysis providing a mechanistic explanation for stroke injuries and metrics due to its ability to model asymmetric interactions among brain regions. Lastly, it revealed the strong influence of SDC in the observed effects.

CRediT authorship contribution statement

Sebastian Idesis: Conceptualization, Formal analysis, Writing – review & editing. **Chiara Favaretto:** Formal analysis. **Nicholas V. Metcalf:** . **Joseph C. Griffis:** . **Gordon L. Shulman:** Conceptualization, Writing – review & editing. **Maurizio Corbetta:** Conceptualization, Writing – review & editing. **Gustavo Deco:** Conceptualization, Writing – review & editing.

Declaration of Competing Interest

The authors declare that they have no known competing financial interests or personal relationships that could have appeared to influence the work reported in this paper.

Data availability

Data will be made available on request.

Appendix A. Supplementary data

Supplementary data to this article can be found online at https://doi.org/10.1016/j.nicl.2022.103233.

References:

Acharya, U.R., Meiburger, K.M., Faust, O., Koh, J.E.W., Oh, S.L., Ciaccio, E.J., Subudhi, A., Jahmunah, V., Sabut, S., 2019. Automatic detection of ischemic stroke using higher order spectra features in brain MRI images. Cognitive systems research 58, 134–142.

Adhikari, M.H., Hacker, C.D., Siegel, J.S., Griffa, A., Hagmann, P., Deco, G., Corbetta, M., 2017. Decreased integration and information capacity in stroke measured by whole brain models of resting state activity. Brain 140 (4), 1068–1085.

Adhikari, M.H., Belloy, M.E., Van der Linden, A., Keliris, G.A., Verhoye, M., 2020. Resting-State Co-activation Patterns as Promising Candidates for Prediction of Alzheimer's Disease in Aged Mice. Front Neural Circuits 14, 612529. https://doi.org/10.3389/fncir.2020.612529.

Adhikari, M.H., Belloy, M.E., Van der Linden, A., Keliris, G.A., Verhoye, M., 2021a. Resting-State Co-activation Patterns as Promising Candidates for Prediction of Alzheimer's Disease in Aged Mice. Frontiers in Neural Circuits 91.

Adhikari, M.H., Griffis, J., Siegel, J.S., Thiebaut de Schotten, M., Deco, G., Instabato, A., Gilson, M., Corbetta, M., 2021b. Effective connectivity extracts clinically relevant prognostic information from resting state activity in stroke. Brain communications 3 (4), fcab233.

Allegra, M., Favaretto, C., Metcalf, N., Corbetta, M., Brovelli, A., 2021. Stroke-related alterations in inter-areal communication. NeuroImage: Clinical 32, 102812.

Arnemann, K.L., Chen, A.-J.-W., Novakovic-Agopian, T., Gratton, C., Nomura, E.M., D'Esposito, M., 2015. Functional brain network modularity predicts response to cognitive training after brain injury. Neurology 84 (15), 1568–1574.

Baldassarre, A., Ramsey, L., Rengachary, J., Zinn, K., Siegel, J.S., Metcalf, N.V., Strube, M.J., Snyder, A.Z., Corbetta, M., Shulman, G.L., 2016. Dissociated functional connectivity profiles for motor and attention deficits in acute right-hemisphere stroke. Brain 139 (7), 2024–2038.

Bates, E., Reilly, J., Wulfeck, B., Dronkers, N., Opie, M., Fenson, J., Kriz, S., Jeffries, R., Miller, L., Herbst, K., 2001. Differential effects of unilateral lesions on language production in children and adults. Brain and language 79 (2), 223–265.

Bayrak, Ş., Khalil, A.A., Villringer, K., Fiebach, J.B., Villringer, A., Margulies, D.S., Ovadia-Caro, S., 2019. The impact of ischemic stroke on connectivity gradients. NeuroImage: Clinical 24, 101947.

Boes, C.J., 2015. History of neurologic examination books. Baylor University Medical Center Proceedings 28 (2), 172–179.

Bowren, M., Bruss, J., Manzel, K., Edwards, D., Liu, C., Corbetta, M., Tranel, D., Boes, A. D., 2022. Post-stroke outcomes predicted from multivariate lesion-behaviour and lesion network mapping. Brain 145 (4), 1338–1353.

Breiman, L., 2001. Random forests. *Machine learning* 45 (1), 5–32.

Broca, P., 1861. Remarques sur le siège de la faculté du langage articulé, suivies d'une observation d'aphémie (perte de la parole). Bulletin et Memoires de la Societe anatomique de Paris 6, 330–357.

Brott, T., Adams Jr., H.P., Olinger, C.P., Marler, J.R., Barsan, W.G., Biller, J., Spilker, J., Holleran, R., Eberle, R., Hertzberg, V., et al., 1989. Measurements of acute cerebral infarction: a clinical examination scale. Stroke 20 (7), 864–870. https://doi.org/10.1161/01.str.20.7.864.

Bullmore, E., Sporns, O., 2009. Complex brain networks: graph theoretical analysis of structural and functional systems. Nature reviews neuroscience 10 (3), 186–198.

Cabral, J., Hugues, E., Kringelbach, M.L., Deco, G., 2012. Modeling the outcome of structural disconnection on resting-state functional connectivity. Neuroimage 62 (3), 1342–1353.

Cabral, J., Kringelbach, M.L., Deco, G., 2017a. Functional connectivity dynamically evolves on multiple time-scales over a static structural connectome: Models and mechanisms. Neuroimage 160, 84–96.

Cabral, J., Vidaurre, D., Marques, P., Magalhães, R., Silva Moreira, P., Miguel Soares, J., Deco, G., Sousa, N., Kringelbach, M.L., 2017b. Cognitive performance in healthy older adults relates to spontaneous switching between states of functional connectivity during rest. Scientific reports 7 (1), 1–13.

Chen, C., Yuan, K., Chu, W.-C.-W., Tong, R.-K.-Y., 2021. The effects of 10 Hz and 20 Hz tACS in network integration and segregation in chronic stroke: a graph theoretical fMRI study. Brain Sciences 11 (3), 377.

Cofré, R., Herzog, R., Mediano, P.A., Piccinini, J., Rosas, F.E., Sanz Perl, Y., Tagliazucchi, E., 2020. Whole-brain models to explore altered states of consciousness from the bottom up. Brain Sciences 10 (9), 626.

Corbetta, M., Ramsey, L., Callejas, A., Baldassarre, A., Hacker, C., Siegel, J., Astafiev, S., Rengachary, J., Zinn, K., Lang, C., Connor, L., Fucetola, R., Strube, M., Carter, A., Shulman, G., 2015. Common behavioral clusters and subcortical anatomy in stroke. Neuron 85 (5), 927–941.

Corbetta, M., Siegel, J.S., Shulman, G.L., 2018. On the low dimensionality of behavioral deficits and alterations of brain network connectivity after focal injury. Cortex 107, 229–237. https://doi.org/10.1016/j.cortex.2017.12.017.

Deco, G., Tononi, G., Boly, M., Kringelbach, M.L., 2015. Rethinking segregation and integration: contributions of whole-brain modelling. Nature reviews neuroscience 16 (7), 430–439.

Deco, G., Kringelbach, M.L., Jirsa, V.K., Ritter, P., 2017. The dynamics of resting fluctuations in the brain: metastability and its dynamical cortical core. Scientific reports 7 (1), 1–14.

Deco, G., Cruzat, J., Cabral, J., Tagliazucchi, E., Laufs, H., Logothetis, N.K., Kringelbach, M.L., 2019. Awakening: Predicting external stimulation to force transitions between different brain states. Proceedings of the National Academy of Sciences 116 (36), 18088–18097. https://www.ncbi.nlm.nih.gov/pmc/arti cles/PMC6731634/pdf/pnas.201905534.pdf.

Favaretto, C., Allegra, M., Deco, G., Metcalf, N.V., Griffis, J.C., Shulman, G.L., Brovelli, A., Corbetta, M., 2022. Subcortical-cortical dynamical states of the human brain and their breakdown in stroke. Nature communications 13 (1).

Foulon, C., Cerliani, L., Kinkingnehun, S., Levy, R., Rosso, C., Urbanski, M., Volle, E., Thiebaut de Schotten, M., 2018. Advanced lesion symptom mapping analyses and implementation as BCBtoolkit. Gigascience 7 (3), giy004.

Friston, K.J., 2011. Functional and effective connectivity: a review. Brain connectivity 1 (1), 13–36.

Friston, K.J., Harrison, L., Penny, W., 2003. Dynamic causal modelling. Neuroimage 19 (4), 1273–1302.

Gilson, M., Moreno-Bote, R., Ponce-Alvarez, A., Ritter, P., Deco, G., Jbabdi, S., 2016. Estimation of directed effective connectivity from fMRI functional connectivity hints at asymmetries of cortical connectome. PLoS computational biology 12 (3), e1004762.

Govindarajan, P., Soundarapandian, R.K., Gandomi, A.H., Patan, R., Jayaraman, P., Manikandan, R., 2020. Classification of stroke disease using machine learning algorithms. Neural Computing and Applications 32 (3), 817–828.

Gratton, C., Nomura, E.M., Pérez, F., D'Esposito, M., 2012. Focal brain lesions to critical locations cause widespread disruption of the modular organization of the brain. Journal of cognitive neuroscience 24 (6), 1275–1285.

Griffis, J. C., Metcalf, N. V., Corbetta, M., & Shulman, G. L. (2019a). Structural disconnections contribute to lesion-induced brain functional connectivity disruptions via direct and indirect mechanisms. *bioRxiv*, 785576.

Griffis, J.C., Metcalf, N.V., Corbetta, M., Shulman, G.L., 2019. Structural Disconnections Explain Brain Network Dysfunction after Stroke. Cell Rep 28 (10), 2527–2540 e2529. https://doi.org/10.1016/j.celrep.2019.07.100.

Griffis, J.C., Metcalf, N.V., Corbetta, M., Shulman, G.L., 2020. Damage to the shortest structural paths between brain regions is associated with disruptions of resting-state functional connectivity after stroke. Neuroimage 210, 116589.

Griffis, J.C., Metcalf, N.V., Corbetta, M., Shulman, G.L., 2021. Lesion Quantification Toolkit: A MATLAB software tool for estimating grey matter damage and white matter disconnections in patients with focal brain lesions. Neuroimage Clin 30, 102639. https://doi.org/10.1016/j.nicl.2021.102639.

Han, X., Jin, H.e., Li, K., Ning, Y., Jiang, L., Chen, P., Liu, H., Zhang, Y., Zhang, H., Tan, Z., Cui, F., Ren, Y.i., Bai, L., Zou, Y., 2020. Acupuncture Modulates Disrupted Whole-Brain Network after Ischemic Stroke: Evidence Based on Graph Theory Analysis. Neural Plasticity 2020, 1–10.

He, B.J., Snyder, A.Z., Vincent, J.L., Epstein, A., Shulman, G.L., Corbetta, M., 2007. Breakdown of functional connectivity in frontoparietal networks underlies behavioral deficits in spatial neglect. Neuron 53 (6), 905–918.

Hejazi, M., Nasrabadi, A.M., 2019. Prediction of epilepsy seizure from multi-channel electroencephalogram by effective connectivity analysis using Granger causality and directed transfer function methods. Cognitive neurodynamics 13 (5), 461–473.

Idesis, S., Faskowitz, J., Betzel, R.F., Corbetta, M., Sporns, O., Deco, G., 2022. Edge-centric analysis of stroke patients: An alternative approach for biomarkers of lesion recovery. NeuroImage: Clinical 103055.

Jobst, B.M., Hindriks, R., Laufs, H., Tagliazucchi, E., Hahn, G., Ponce-Alvarez, A., Stevner, A.B.A., Kringelbach, M.L., Deco, G., 2017. Increased Stability and Breakdown of Brain Effective Connectivity During Slow-Wave Sleep: Mechanistic Insights from Whole-Brain Computational Modelling. Scientific reports 7 (1), 4634. https://doi.org/10.1038/s41598-017-04522-x.

Karnath, H.-O., Sperber, C., Rorden, C., 2018. Mapping human brain lesions and their functional consequences. Neuroimage 165, 180–189.

Kringelbach, M.L., McIntosh, A.R., Ritter, P., Jirsa, V.K., Deco, G., 2015. The rediscovery of slowness: exploring the timing of cognition. Trends in cognitive sciences 19 (10), 616–628.

Kringelbach, M.L., Cruzat, J., Cabral, J., Knudsen, G.M., Carhart-Harris, R., Whybrow, P. C., Logothetis, N.K., Deco, G., 2020. Dynamic coupling of whole-brain neuronal and neurotransmitter systems. Proceedings of the National Academy of Sciences 117 (17), 9566–9576.

Kuznetsov, Y.A., 1998. Elements of applied bifurcation theory. Applied mathematical sciences 112, 591.

Margulies, D.S., Ghosh, S.S., Goulas, A., Falkiewicz, M., Huntenburg, J.M., Langs, G., Bezgin, G., Eickhoff, S.B., Castellanos, F.X., Petrides, M., Jefferies, E., Smallwood, J., 2016. Situating the default-mode network along a principal gradient of macroscale cortical organization. Proceedings of the National Academy of Sciences 113 (44), 12574–12579.

Mesulam, M.M., 1981. A cortical network for directed attention and unilateral neglect. Annals of Neurology: Official Journal of the American Neurological Association and the Child Neurology Society 10 (4), 309–325.

Meunier, D., Lambiotte, R., Bullmore, E.T., 2010. Modular and hierarchically modular organization of brain networks. Frontiers in neuroscience 4, 200.

Mitra, A., Raichle, M.E., 2016. How networks communicate: propagation patterns in spontaneous brain activity. Philosophical Transactions of the Royal Society B: Biological Sciences 371 (1705), 20150546.

Mitra, A., Snyder, A.Z., Hacker, C.D., Pahwa, M., Tagliazucchi, E., Laufs, H., Leuthardt, E. C., Raichle, M.E., 2016. Human cortical–hippocampal dialogue in wake and slow-wave sleep. Proceedings of the National Academy of Sciences 113 (44), E6868. E6876.

Newman, M.E., Girvan, M., 2004. Finding and evaluating community structure in networks. Phys Rev E Stat Nonlin Soft Matter Phys 69 (2 Pt 2), 026113. https://doi. org/10.1103/PhysRevE.69.026113.

Ovadia-Caro, S., Villringer, K., Fiebach, J., Jungehulsing, G.J., Van Der Meer, E., Margulies, D.S., Villringer, A., 2013. Longitudinal effects of lesions on functional networks after stroke. Journal of Cerebral Blood Flow & Metabolism 33 (8), 1279–1285.

Pallarés, V., Insabato, A., Sanjuán, A., Kühn, S., Mantini, D., Deco, G., Gilson, M., 2018. Extracting orthogonal subject-and condition-specific signatures from fMRI data using whole-brain effective connectivity. Neuroimage 178, 238–254.

Park, H.-J., Friston, K., 2013. Structural and functional brain networks: from connections to cognition. Science 342 (6158).

Pini, L., Salvalaggio, A., De Filippo De Grazia, M., Zorzi, M., Thiebaut de Schotten, M., Corbetta, M., 2021. A novel stroke lesion network mapping approach: improved accuracy yet still low deficit prediction. Brain communications 3 (4).

Power, J.D., Schlaggar, B.L., Lessov-Schlaggar, C.N., Petersen, S.E., 2013. Evidence for hubs in human functional brain networks. Neuron 79 (4), 798–813.

Raut, R.V., Snyder, A.Z., Raichle, M.E., 2020. Hierarchical dynamics as a macroscopic organizing principle of the human brain. Proceedings of the National Academy of Sciences 117 (34), 20890–20897.

Saenger, V.M., Ponce-Alvarez, A., Adhikari, M., Hagmann, P., Deco, G., Corbetta, M., 2018. Linking Entropy at Rest with the Underlying Structural Connectivity in the Healthy and Lesioned Brain. Cerebral Cortex 28 (8), 2948–2958. https://doi.org/ 10.1093/cercor/bhx176.

Salvalaggio, A., De Filippo De Grazia, M., Zorzi, M., Thiebaut de Schotten, M., Corbetta, M., 2020. Post-stroke deficit prediction from lesion and indirect structural and functional disconnection. Brain 143 (7), 2173–2188.

Sanz Perl, Y., Pallavicini, C., Pérez Ipiña, I., Demertzi, A., Bonhomme, V., Martial, C., Panda, R., Annen, J., Ibañez, A., Kringelbach, M., Deco, G., Laufs, H., Sitt, J., Laureys, S., Tagliazucchi, E., Taylor, P.N., 2021. Perturbations in dynamical models of whole-brain activity dissociate between the level and stability of consciousness. PLoS computational biology 17 (7), e1009139.

Schaefer, A., Kong, R., Gordon, E.M., Laumann, T.O., Zuo, X.-N., Holmes, A.J., Eickhoff, S.B., Yeo, B.T., 2018. Local-global parcellation of the human cerebral cortex from intrinsic functional connectivity MRI. Cerebral Cortex 28 (9), 3095–3114.

Siegel, J.S., Ramsey, L.E., Snyder, A.Z., Metcalf, N.V., Chacko, R.V., Weinberger, K., Baldassarre, A., Hacker, C.D., Shulman, G.L., Corbetta, M., 2016. Disruptions of network connectivity predict impairment in multiple behavioral domains after stroke. E4376 Proc Natl Acad Sci U S A 113 (30), E4367. https://doi.org/10.1073/ pnas.1521083113.

Siegel, J.S., Seitzman, B.A., Ramsey, L.E., Ortega, M., Gordon, E.M., Dosenbach, N.U., Petersen, S.E., Shulman, G.L., Corbetta, M., 2018. Re-emergence of modular brain networks in stroke recovery. Cortex 101, 44–59.

Sporns, O., 2013. Network attributes for segregation and integration in the human brain. Curr Opin Neurobiol 23 (2), 162–171. https://doi.org/10.1016/j.conb.2012.11.015.

Sprigg, N., Gray, L.J., Bath, P.M.W., Lindenstrøm, E., Boysen, G., De Deyn, P.P., Friis, P., Leys, D., Marttila, R., Olsson, J.-E., O'Neill, D., Ringelstein, E.B., van der Sande, J.-J., Turpie, A.G.G., 2007. Stroke severity, early recovery and outcome are each related with clinical classification of stroke: data from the 'Tinzaparin in Acute Ischaemic Stroke Trial'(TAIST). Journal of the neurological sciences 254 (1-2), 54–59.

Sun, J., Wang, D., Chen, S., Pang, R., Liu, H., Wang, J., Zhang, Y., Wang, G., Yang, A., 2021. The behavioral significance of resting state network after stroke: A study via graph theory analysis with near-infrared spectroscopy. Medicine in Novel Technology and Devices 11, 100083.

Tononi, G., Sporns, O., Edelman, G.M., 1994. A measure for brain complexity: relating functional segregation and integration in the nervous system. Proceedings of the National Academy of Sciences 91 (11), 5033–5037.

Tzourio-Mazoyer, N., Landeau, B., Papathanassiou, D., Crivello, F., Etard, O., Delcroix, N., Mazoyer, B., Joliot, M., 2002. Automated anatomical labeling of activations in SPM using a macroscopic anatomical parcellation of the MNI MRI single-subject brain. Neuroimage 15 (1), 273–289.

van den Heuvel, M.P., Sporns, O., 2013. Network hubs in the human brain. Trends in cognitive sciences 17 (12), 683–696.

Vecchio, F., Caliandro, P., Reale, G., Miraglia, F., Piludu, F., Masi, G., Iacovelli, C., Simbolotti, C., Padua, L., Leone, E., Alù, F., Colosimo, C., Rossini, P.M., 2019a. Acute cerebellar stroke and middle cerebral artery stroke exert distinctive modifications on functional cortical connectivity: A comparative study via EEG graph theory. Clinical Neurophysiology 130 (6), 997–1007.

Vecchio, F., Tomino, C., Miraglia, F., Iodice, F., Erra, C., Di Iorio, R., Judica, E., Alù, F., Fini, M., Rossini, P.M., 2019b. Cortical connectivity from EEG data in acute stroke: A study via graph theory as a potential biomarker for functional recovery. International Journal of Psychophysiology 146, 133–138.

Wang, X., Seguin, C., Zalesky, A., Wong, W.-W., Chu, W.-C.-W., Tong, R.-K.-Y., 2019. Synchronization lag in post stroke: relation to motor function and structural connectivity. Network Neuroscience 3 (4), 1121–1140.

Warren, D.E., Power, J.D., Bruss, J., Denburg, N.L., Waldron, E.J., Sun, H., Petersen, S.E., Tranel, D., 2014. Network measures predict neuropsychological outcome after brain injury. Proceedings of the National Academy of Sciences 111 (39), 14247–14252.

Wei, L., Wu, G.-R., Bi, M., Baeken, C., 2021. Effective connectivity predicts cognitive empathy in cocaine addiction: a spectral dynamic causal modeling study. Brain Imaging and Behavior 15 (3), 1553–1561.

Weiss Cohen, M., Regazzoni, D., 2020. Hand rehabilitation assessment system using leap motion controller. Ai & Society 35 (3), 581–594.

Wodeyar, A., Cassidy, J.M., Cramer, S.C., Srinivasan, R., 2020. Damage to the structural connectome reflected in resting-state fMRI functional connectivity. Network Neuroscience 4 (4), 1197–1218.

Yeh, F.-C., Panesar, S., Fernandes, D., Meola, A., Yoshino, M., Fernandez-Miranda, J.C., Vettel, J.M., Verstynen, T., 2018. Population-averaged atlas of the macroscale human structural connectome and its network topology. Neuroimage 178, 57–68.

Yeh, F.-C., Tseng, W.-Y.-I., 2011. NTU-90: a high angular resolution brain atlas constructed by q-space diffeomorphic reconstruction. Neuroimage 58 (1), 91–99.

Yeo, B.T., Krienen, F.M., Sepulcre, J., Sabuncu, M.R., Lashkari, D., Hollinshead, M., Roffman, J.L., Smoller, J.W., Zöllei, L., Polimeni, J.R., 2011. The organization of the human cerebral cortex estimated by intrinsic functional connectivity. Journal of neurophysiology.